

Tunable Kondo screening length at a Y-junction of three inhomogeneous spin chains.

Domenico Giuliano^{a,b,*}, Andrea Nava^{a,b}, Pasquale Sodano^c

^a*Dipartimento di Fisica, Università della Calabria, Arcavacata di Rende I-87036, Cosenza, Italy*

^b*INFN, Gruppo collegato di Cosenza, Arcavacata di Rende I-87036, Cosenza, Italy*

^c*I.N.F.N., Sezione di Perugia, Via A. Pascoli, I-06123, Perugia, Italy*

Abstract

We derive the topological Kondo Hamiltonian describing a Y junction of three XX-spin chains connected to outer quantum Ising chains with different tilting angles for the Ising axis. We show that the tilting angles in the spin models play the role of the phases of the superconducting order parameters at the interfaces between bulk superconductors and one-dimensional conducting normal electronic wires. As a result, different tilting angles induce nonzero equilibrium spin (super)currents through the junction. Employing the renormalization group approach to the topological Kondo model, we derive the scaling formulas for the equilibrium spin currents. We argue that, by monitoring the crossover in the currents induced by the Kondo effect, it is possible to estimate the Kondo screening length. In particular, we prove how it is possible to tune the Kondo length by acting on the applied phases only; this enables us to map out the scaling properties by just tuning the tilting angles and the Kondo length accordingly.

Keywords: Spin chain models, Scattering mechanisms and Kondo effect, Fermions in reduced dimensions, Kosterlitz-Thouless transition: magnetic systems

PACS: 75.10.Pq, 72.15.Qm, 71.10.Pm, 75.30.Kz

1. Introduction

In its original description, the Kondo effect was evidenced as a low-temperature upturn in the resistance of a metal containing magnetic impurities antiferromagnetically interacting with the spin of the itinerant conduction electrons in the metal (the “Kondo interaction”) [1, 2, 3].

The effect is determined by the low-energy/low-temperature T proliferation of impurity spin-flip processes. These induce a nonperturbative, strongly correlated, (“Kondo”) state in which the electron spins cooperate to “dynamically screen” the impurity spin. Letting s be the impurity spin and k be the number of different electronic spin screening channels, if $k = 2s$, the impurity spin is perfectly screened and the Nozières Fermi-liquid state sets in the $T \rightarrow 0$ limit, in which the

*Corresponding author

Email addresses: domenico.giuliano@fis.unical.it (Domenico Giuliano), andrea_nava@msn.com (Andrea Nava), pasquale.sodano01@gmail.com (Pasquale Sodano)

impurity effectively acts as a spinless localized scatterer (the “Kondo singlet”) [4, 5]. Instead, when $k > 2s$ (“overscreened Kondo effect”), a non Fermi-liquid state with rather peculiar properties sets in [6, 7].

Right after its explanation [1], the Kondo effect appeared as a paradigmatic example of a many-body correlated electronic state, eventually becoming a testground both for theoretical many-body techniques [8], and for designing correlated electronic nanodevices [3]. In particular, the possibility of realizing the effect in controlled systems with tunable parameters, such as quantum dots with metallic [9, 10, 11, 12, 13], or superconducting leads [14, 15, 16], allowed for engineering quantum circuits with the maximum value for the conductance per each single channel [3]. Moreover, a recent, remarkable achievement has been provided by the realization of a peculiar, overscreened “topological” Kondo effect (TKE), in which the Kondo impurity is determined by the Majorana fermionic modes arising at the endpoints of one-dimensional (1D) topological superconductors [17, 18, 19, 20].

A key feature of the Kondo effect, that is strictly related to its nonperturbative nature, is the emergence of a finite temperature scale T_K (the “Kondo temperature”) separating the high- T perturbative regime from the $T \rightarrow 0$ Kondo fixed point. Specifically, T_K emerges within the perturbative renormalization group (RG) framework, as a dimensionful scale that is invariant along the RG trajectories [21, 4].

Using the Fermi velocity v associated to itinerant electrons, it is possible to trade T_K for a length scale $\ell_K \sim v/T_K$. The physical meaning of ℓ_K is that the value of any local observable at a distance x from the impurity is determined by the Kondo fixed point if $x < \ell_K$, while it only takes perturbative correction in the Kondo interaction if $x > \ell_K$. Basically, ℓ_K measures the size of the spin cloud dynamically screening the impurity spin (the “Kondo cloud”), and is accordingly dubbed as the “Kondo screening length” (KL), an analog of which has also been proposed to emerge at a Majorana mode coupled to a 1D quantum wire [22]. The emergence of ℓ_K is a direct consequence of the implementation of the scaling assumption in the Kondo regime [21].

Finding an experimental evidence of ℓ_K would be a strong confirmation of the validity of the scaling assumption. Despite the strong theoretical background supporting the existence of the KL, so far it has never been experimentally detected. Such a failure may be attributed to a number of reasons, such as the tiny value of spin correlations over distances of the order of ℓ_K , the finite density of magnetic impurities in a real metal, the effects of the interaction between itinerant electrons, etc. [23].

A promising route to overcome the difficulties in measuring ℓ_K is realizing the Kondo effect in nonconducting systems, such as quantum spin chains (SCs). Indeed, despite typically being insulating, spin-1/2 quantum SCs have a low-lying elementary excitation spectrum consisting of spin-1/2 delocalized “spinons”, collective modes carrying spin but no charge, which can effectively screen an isolated magnetic impurity antiferromagnetically coupled to the chain [24, 25, 26, 27]. Lattice spin correlations in real space are typically more easily measurable than spin density correlations between distant electrons in a metal, which makes spin chains a pretty better arena to probe ℓ_K , compared to metals. In addition, working with spin chains allows for studying Kondo physics by using a series of tools developed for spin systems, such as entanglement witnesses and negativity [28, 29]. Remarkably, nowadays technology allows for realizing systems behaving as quantum SCs with tunable parameters by using, for instance, cold atoms on an optical lattice [30, 31, 32],

or pertinently engineered Josephson junction one-dimensional arrays [33, 34]. In this case, the Kondo problem formally emerges by using the Jordan-Wigner (JW) representation for the spin $1/2$ operators to map the lattice spin Hamiltonian onto a Luttinger liquid model interacting with an isolated magnetic impurity [31, 32, 35].

Working with a Y-junction of quantum spin chains (YSC), allows for the realization of Kondo Hamiltonians even without explicitly introducing a quantum impurity in the chains. Indeed, when implementing the JW transformation for a YSC, in order to preserve the correct (anti)commutation relations between spin operators belonging to different chains, we have to introduce as many additional real fermionic degrees of freedom (the "Klein factors" (KFs)) as many chains [36]. The KFs do now appear in the bulk Hamiltonian of the chains, as they have to, but, when introduced in the boundary interaction Hamiltonian describing the junction, they determine an effective, spin- $1/2$ degree of freedom, interacting with the bulk degrees of freedom of the chains through a topological Kondo Hamiltonian, with the bulk spin density operator being a nonlocal function of the single chains. By now, a topological Kondo Hamiltonian has been shown to describe a junction of three quantum Ising chains [37, 38], of three XX chains [36], of a pertinently engineered Josephson junction network [34], and of three XY chains, continuously interpolating between the Ising- and the XX-limit [39].

As a possible route to estimate ℓ_K at a YSC, it has been proposed to look at the scaling of a pertinently defined local magnetization at the junction [34, 39]. However, it would be much more effective to directly extract scaling properties from a (spin, in this case) current transport measurement, as it is typically done with Kondo effect in a quantum dot with metallic leads. In fact, measuring the equilibrium (super)current pattern induced through similar junctions realized with Josephson junction arrays connected to bulk superconductors at fixed phases, has provided an effective mean to monitor the phase diagram of the junction and the associated scaling properties [33, 40, 41, 42]. An important step in extending this approach to a YSC has recently been provided in Ref.[43], where it has been shown how, when applying the JW transformation to the interface between an XX-chain and a quantum Ising chain with Ising axis rotated with respect to the z -axis (in spin space) of the XX-chain, the interface is mapped onto the interface between a spinless normal 1D conductor and a p-wave superconductor, with the phase of the order parameter equal to twice the tilting angle of the Ising axis. In the low-energy, long-wavelength limit, once the system parameters are pertinently chosen, an interface as such stabilizes perfect Andreev reflection on the normal side, which is the same as connecting a "truly" fermionic system to a bulk superconductor at fixed phase. As a result, this becomes an effective mechanism to induce an equilibrium, nonzero spin current pattern across the YSC.

In this paper we first develop an effective field theory describing the low-energy, long-wavelength limit of a junction of N XX-spin chains connected to "outer" quantum Ising chains with different tilting angles for the Ising axis. Therefore, we use the result to analyze the scaling properties of the TKE arising at a three-chain junction.

Technically, we argue how, in perfect analogy with the derivation done in Refs.[44, 45] for a normal metal-superconductor interface, for a long enough XX-chains, each terminal Ising chain may be traded for a pertinent boundary interaction Hamiltonian, only depending on an emerging Majorana mode γ and on the tilting angle of the corresponding Ising axis. In the low-energy, long-wavelength limit, we prove that the emerging Majorana mode stabilizes perfect Andreev reflection

for JW fermions at the interface, with a phase shift equal to twice the tilting angle of the Ising axis. As a result, the different tilting angles of the Ising chains work as applied phases at the endpoints of the XX-chains, thus inducing a nonzero equilibrium spin current pattern across the junction.

To describe how the spin currents are affected by the TKE, we first map our system onto a Y junction of three quantum Ising chains, with, in general, boundary couplings all different from each other, and all explicitly depending on the applied phases. Therefore, combining the RG approach to the (anisotropic) TKE, which eventually provides the running couplings as functions of the bare couplings and of the running scale, with the functional dependence of the bare couplings on the applied phases, we recover the running couplings as a function of the applied phases. This allows us to derive scaling formulas for the system groundstate energy and, by differentiating the energy with respect to the applied phases, to derive scaling formulas for the spin currents across the junction.

Compared to the expected scaling of the currents as the first inverse power of the length of the leads ℓ [46, 47, 33, 48, 49], the TKE induces a crossover in the form of an upturn in the currents as $\ell \sim \ell_K$. Probing such a crossover would on one hand provide a direct evidence of the emergence of the TKE at the YSC, on the other hand it would yield a direct measurement of ℓ_K .

In addition, we prove that ℓ_K itself is a known function of the applied phases, whose functional form can be readily inferred from the explicit solution of the RG equations for the running couplings. In fact, this is possibly the main advantage of measuring ℓ_K in our YSC, compared to other Kondo systems. Acting on the applied phases, we may tune in a controlled way the bare couplings and, therefore, we may in principle tune ℓ_K at will. So, ℓ_K itself becomes a *tunable parameter*, which we may act on by pertinently varying the applied phases, that is, the tilting angles of the Ising axes.

This result eventually leads to two complementary ways to probe ℓ_K in our system. Indeed, it is possible to either look at the scaling of the currents with ℓ at fixed applied phases, or to alternatively fix ℓ and vary the phases by, therefore, tuning ℓ_K accordingly. In particular, the second method allows for recovering the scaling by tuning ℓ_K , *without changing* ℓ , which is the hardest thing to achieve in a real-life system.

The paper is organized as follows:

- In Sec.2 we introduce the model Hamiltonian for a junction of N spin chains connected to each other at one of their endpoints. Each chain is modeled as an “inner” quantum XX-chain of length ℓ connected at an “outer” quantum Ising chain with a tilted Ising axis. Eventually, consistently with the derivation of Refs.[44, 45] we trade the outer chains for pertinent boundary Hamiltonians localized at the interfaces;
- In Sec.3 we introduce our method for computing the spin current using the simple example of the $N = 2$ junction at fixed applied phases. This is equivalent to a single, inhomogeneous spin chain and, therefore, in principle it does not require introducing KFs to resort to JW fermions. For this reason, we extensively use the $N = 2$ chain as a testground of our method, showing how it enables us to recover all the known results for a single chain connected to two superconductors at fixed phase difference [46, 47, 33];

- In Sec.4 we extend the derivation of Sec.3 to the $N = 3$ junction, particularly evidencing the emergence of the KFs in the boundary Hamiltonian describing the junction;
- In Sec.5 we derive the RG equations for the running boundary couplings in the $N = 3$ junction;
- In Sec.6 we use the results of Sec.5 to derive the spin current pattern at the onset of the Kondo regime, showing the explicit dependence of ℓ_K on the applied phases and, therefore, its tunability, in some simple cases in which it can be explicitly derived in a closed-form;
- In Sec.7 we summarize the main results of our work;
- We provide the mathematical details of our derivation in the various Appendices.

2. Model Hamiltonian for the junction of N spin chains

According to Ref.[43] we describe each quantum spin chain by means of a one-dimensional, inhomogeneous lattice quantum spin Hamiltonian H_{SC}^λ over an L site lattice with open boundary conditions at the endpoint at $j = L$. Therefore, denoting with λ the chain index, we set

$$H_{\text{SC}}^\lambda = - \sum_{j=1}^{L-1} \{ (t_j + \gamma_j) \hat{\sigma}_{j,\lambda}^m \hat{\sigma}_{j+1,\lambda}^m + (t_j - \gamma_j) \hat{\sigma}_{j,\lambda}^n \hat{\sigma}_{j+1,\lambda}^n \} - \sum_{j=1}^L g_j \sigma_{j,\lambda}^z \quad , \quad (1)$$

with the parameters chosen as detailed below:

- The isotropic contribution to the magnetic exchange t_j :

$$t_j = \begin{cases} J & , (1 \leq j \leq \ell - 1) \\ J' & , (j = \ell) \\ t & , (\ell + 1 \leq j \leq L - 1) \end{cases} \quad ; \quad (2)$$

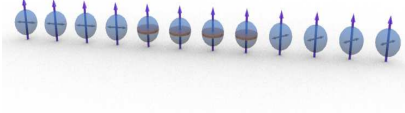
- The anisotropic contribution to the magnetic exchange γ_j :

$$\gamma_j = \begin{cases} 0 & , (1 \leq j \leq \ell) \\ \gamma & , (\ell + 1 \leq j \leq L - 1) \end{cases} \quad ; \quad (3)$$

- The applied transverse field g_j :

$$g_j = \begin{cases} H & , (1 \leq j \leq \ell) \\ g & , (\ell + 1 \leq j \leq L) \end{cases} \quad ; \quad (4)$$

a)



b)

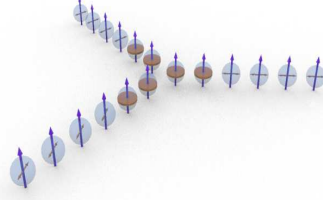


Figure 1: **a)** Sketch of a single chain with inhomogeneous parameters corresponding (via the Jordan-Wigner transformation) to a spinless, SNS junction. Following the drawing code of Ref.[43], each sphere represents a quantum spin. Spheres with the equatorial plane colored in red represent spins interacting with an isotropic magnetic interaction lying within the XY-plane in spin space (the XX-part of the whole chain), while spheres with just one colored segment within the equatorial plane correspond to spins with an Ising interaction directed along the segment. The tilting angle between the Ising interaction axes in the two external leads is mapped onto the phase difference between the superconducting leads of the SNS junction; **b)** Sketch of the $N = 3$ junction analyzed in the paper, realized with three inhomogeneous spin chains, each one consisting of an (inner) XX-part joined to an (outer) Ising part, with the applied phases to each chain defined by the direction of the Ising interaction between the spins.

- The (in-plane) projected spin operators:

$$\begin{aligned}\hat{\sigma}_{j,\lambda}^m &= \hat{m}_{j,\lambda} \cdot \vec{\sigma}_{j,\lambda} = \cos(\phi_{j,\lambda})\sigma_{j,\lambda}^x + \sin(\phi_{j,\lambda})\sigma_{j,\lambda}^y = e^{-i\phi_{j,\lambda}}\sigma_{j,\lambda}^+ + e^{i\phi_{j,\lambda}}\sigma_{j,\lambda}^- \\ \hat{\sigma}_{j,\lambda}^n &= \hat{n}_{j,\lambda} \cdot \vec{\sigma}_{j,\lambda} = -\sin(\phi_{j,\lambda})\sigma_{j,\lambda}^x + \cos(\phi_{j,\lambda})\sigma_{j,\lambda}^y = -ie^{-i\phi_{j,\lambda}}\sigma_{j,\lambda}^+ + ie^{i\phi_{j,\lambda}}\sigma_{j,\lambda}^- \quad ,\end{aligned}\quad (5)$$

with

$$\phi_{j,\lambda} = \begin{cases} 0 & , \quad 1 \leq j \leq \ell \\ \phi_\lambda & , \quad \ell + 1 \leq j \leq L \end{cases} \quad (6)$$

(note that, differently from all the other parameters, to induce a nonzero spin current pattern through the junction, we choose the phase ϕ to be dependent on the chain index λ).

The chains are connected to each other at the $j = 1$ endpoint. This defines the actual junction, which is described by the boundary Hamiltonian H_Δ , given by

$$H_\Delta = -J_\Delta \sum_{\lambda=1}^N \{ \sigma_{1,\lambda}^x \sigma_{1,\lambda+1}^x + \sigma_{1,\lambda}^y \sigma_{1,\lambda+1}^y \} \quad , \quad (7)$$

with N being the number of chains and $\lambda + N \equiv \lambda$.

In Fig.1, we provide a sketch of a single, inhomogeneous chain, and of the junction with $N = 3$ chain, to which we devote our attention in this paper.

The equilibrium spin current through a chain is obtained as the average of the z -component of the spin current density operator, $J_{[j,j+1];\lambda}^z$. This is a link operator, which can be derived from the continuity equation for the spin density operator at a site j ($1 \leq j < \ell$). Indeed, from the Heisenberg equations of motion for the lattice spin operator, we obtain

$$\partial_t \sigma_{j,\lambda}^z = -i[\sigma_{j,\lambda}^z, H_{\text{SC},\lambda}] = J_{[j,j+1];\lambda}^z - J_{[j-1,j];\lambda}^z \quad , \quad (8)$$

with

$$J_{[j,j+1];\lambda}^z = J \{ \sigma_{j,\lambda}^x \sigma_{j+1,\lambda}^y - \sigma_{j,\lambda}^y \sigma_{j+1,\lambda}^x \} \quad . \quad (9)$$

To map the quantum spin-1/2 spin chain onto an equivalent spinless fermion model, we employ the generalized JW transformation introduced in Ref.[36]. This requires introducing as many KFs η_λ as many chains, and setting [36, 37, 34, 39]

$$\begin{aligned} \sigma_{j,\lambda}^+ &= i\eta_\lambda c_{j,\lambda}^\dagger e^{i\pi \sum_{t=1}^{j-1} c_{t,\lambda}^\dagger c_{t,\lambda}} \\ \sigma_{j,\lambda}^- &= i\eta_\lambda c_{j,\lambda} e^{i\pi \sum_{t=1}^{j-1} c_{t,\lambda}^\dagger c_{t,\lambda}} \\ \sigma_{j,\lambda}^z &= c_{j,\lambda}^\dagger c_{j,\lambda} - \frac{1}{2} \quad . \end{aligned} \quad (10)$$

In Eq.(10), $\{c_{j,\lambda}, c_{j,\lambda}^\dagger\}$ ($j = 1, \dots, L; \lambda = 1, \dots, N$) is a set of $L \times N$ spinless lattice fermion operators, while the Klein factors η_λ are fermion operators satisfying the anticommutation algebra

$$\begin{aligned} \{\eta_\lambda, \eta_{\lambda'}\} &= 2\delta_{\lambda,\lambda'} \\ \{\eta_\lambda, c_{j,\lambda'}\} &= \{\eta_\lambda, c_{j,\lambda'}^\dagger\} = 0 \quad . \end{aligned} \quad (11)$$

Upon inserting the JW formulas into the (“bulk”) Hamiltonian operators in Eq.(1) the Klein factors cancel. The corresponding Hamiltonian for the λ -chain is given by

$$\begin{aligned} H_{\text{SC}}^\lambda &= -J \sum_{j=1}^{\ell-1} \{c_{j,\lambda}^\dagger c_{j+1,\lambda} + c_{j+1,\lambda}^\dagger c_{j,\lambda}\} - H \sum_{j=1}^{\ell} c_{j,\lambda}^\dagger c_{j,\lambda} - J' \{c_{\ell,\lambda}^\dagger c_{\ell+1,\lambda} + c_{\ell+1,\lambda}^\dagger c_{\ell,\lambda}\} \\ &\quad - t \sum_{j=\ell+1}^{L-1} \{c_{j,\lambda}^\dagger c_{j+1,\lambda} + c_{j+1,\lambda}^\dagger c_{j,\lambda}\} - \gamma \sum_{j=\ell+1}^{L-1} \{c_{j,\lambda} c_{j+1,\lambda} e^{-2i\phi_\lambda} + c_{j+1,\lambda}^\dagger c_{j,\lambda}^\dagger e^{2i\phi_\lambda}\} - g \sum_{j=\ell+1}^L c_{j,\lambda}^\dagger c_{j,\lambda} \quad (12) \end{aligned}$$

In terms of JW fermions, the right-hand side of Eq.(12) describes a junction between a normal wire (ranging from $j = 1$ to $j = \ell$), and a p-wave topological superconductor (ranging from $j = \ell + 1$ to $j = L$).

To further simplify our derivation, in the following we employ the “long- ℓ ” approximation of Refs.[44, 45], by trading the lead Hamiltonian in Eq.(12) for a simple boundary Hamiltonian depending on the degrees of freedom in the “normal” part of the chain [44, 45], as well as on the emerging, “Majorana-like” zero-mode operator at the endpoint of the superconducting lead [50]. To better ground such an approximation, in Appendix Appendix A, we exactly derive the boundary Hamiltonian in the limit $\gamma = t$ and $g = 0$ on the ”p-wave” side of the junction (that, for the chain λ , is given by $H_{\text{F},\lambda}$ in Eq.(A.6) of Appendix Appendix A). As a result, the “bulk” Hamiltonian of the system in fermionic representation takes the form [50]

$$H_{\text{Bulk}} = \sum_{\lambda=1}^N H_{\text{F},\lambda} = \sum_{\lambda=1}^N \left\{ -J \sum_{j=1}^{\ell-1} [c_{j,\lambda}^\dagger c_{j+1,\lambda} + c_{j+1,\lambda}^\dagger c_{j,\lambda}] - H \sum_{j=1}^{\ell} c_{j,\lambda}^\dagger c_{j,\lambda} + i\frac{\tau}{2} \gamma_\lambda [e^{-i\phi_\lambda} c_{\ell,\lambda} + e^{i\phi_\lambda} c_{\ell,\lambda}^\dagger] \right\} \quad , \quad (13)$$

with τ and the real, zero-energy Majorana mode γ_λ defined in Appendix Appendix A.

Resorting to the JW fermion for H_Δ , we obtain

$$H_\Delta = J_\Delta \sum_{\lambda=1}^N [i\eta_\lambda \eta_{\lambda+1}] \{i[c_{1,\lambda}^\dagger c_{1,\lambda+1} - c_{1,\lambda+1}^\dagger c_{1,\lambda}]\} \quad , \quad (14)$$

with, again, $\lambda + N \equiv \lambda$. Eq.(14) shows that, differently from what happens with H_{Bulk} , the KFs do contribute to H_Δ . In particular, for $N = 3$ we obtain a special case of the topological Kondo Hamiltonian at a junction of the three quantum spin [37, 34, 39].

Once expressed in terms of JW fermions, the current density $j_{[j,j+1];\lambda}^z$ is given by

$$j_{[j,j+1];\lambda}^z = -2iJ \{c_{j,\lambda}^\dagger c_{j+1,\lambda} - c_{j+1,\lambda}^\dagger c_{j,\lambda}\} \quad . \quad (15)$$

Using the continuity equation over the link $[\ell, \ell + 1]$, we eventually find that, under stationary conditions, the average value of $j_{[j,j+1];\lambda}^z$ is the same as the average value, over the reference state, of the operator I_λ , defined as

$$I_\lambda = \frac{\tau}{2} \gamma_\lambda \{e^{-i\phi_\lambda} c_{\ell,\lambda} - e^{i\phi_\lambda} c_{\ell,\lambda}^\dagger\} = \frac{\partial H_{B,\lambda}}{\partial \phi_\lambda} \quad . \quad (16)$$

Eq.(16) provides a straightforward way to derive the equilibrium current pattern through the junction by just differentiating the groundstate energy with respect to the applied phases. Therefore, in the following we systematically use Eq.(16) to evaluate the currents.

Before concluding this Section, it is worth stressing how, in general, we expect that the periodicity of the spin equilibrium current through a chain depends on whether the number of site ℓ is even, or odd. The analysis of the even-odd chains is detailed in Appendix [Appendix B](#). For the sake of simplicity, in the following we will be focusing onto the even- ℓ case only.

3. Spin supercurrent through the $N = 2$ -junction

Before analyzing the $N = 3$ YSC, in this Section we illustrate our approach to computing the equilibrium spin current using the example of the $N = 2$ junction. Indeed, the junction between two spin chains is equivalent to a single, inhomogeneous spin chain, with the Hamiltonian being exactly solvable, with no need of introducing the KFs.

In JW fermionic coordinates, the $N = 2$ junction Hamiltonian, $H_\Delta^{(2)}$, is given by

$$H_\Delta^{(2)} = J_\Delta [i\eta_1 \eta_2] \{i[c_{1,1}^\dagger c_{1,2} - c_{1,2}^\dagger c_{1,1}]\} \quad , \quad (17)$$

with the bulk Hamiltonian $H_{\text{Bulk}}^{(2)} = \sum_{\lambda=1,2} H_{\text{SC}}^\lambda$, and H_{SC}^λ given in Eq.(12).

$H_\Delta^{(2)}$ in Eq.(17) is the only term, in the junction Hamiltonian, containing the KF's in the product $i\eta_1 \eta_2$. Rewriting this operator as $2\xi^\dagger \xi - 1$, with $\xi = \frac{\eta_1 + i\eta_2}{2}$, we see that it commutes with the whole Hamiltonian and that its eigenvalues are ± 1 . Accordingly, for all the practical purposes, it can be dropped from $H_\Delta^{(2)}$ and substituted with ± 1 . As a double check of the conclusion that KFs are unessential for $N = 2$, we should verify that the final result for the equilibrium spin supercurrent is independent of the sign of J_Δ .

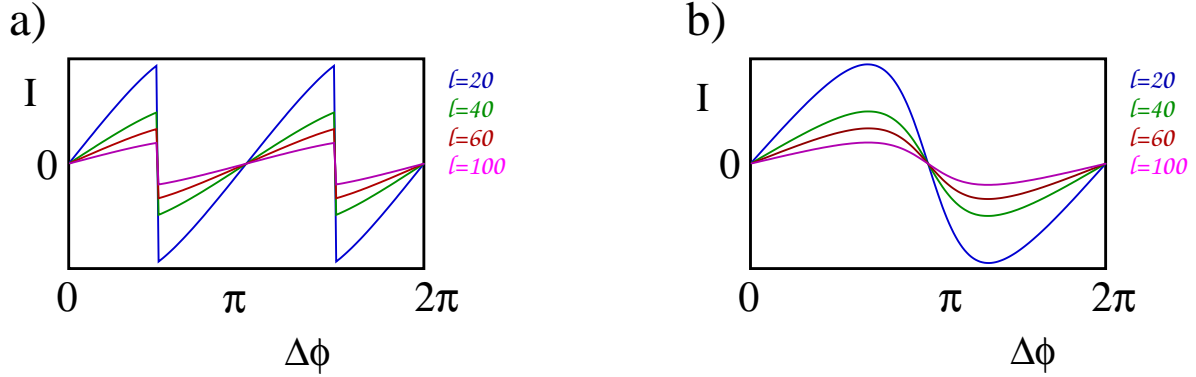


Figure 2: **a)** $I[\Delta\phi]$ as a function of $\Delta\phi$ through an $N = 2$ -junction with $J = 1$ computed by exact diagonalization with $J_\Delta = 0.4$, $\tau = 1$, $\mu = 0.05$, and $\ell = 20$ (blue curve), $\ell = 40$ (green curve), $\ell = 60$ (red curve), $\ell = 100$ (magenta curve). At fixed J_Δ basically the curve collapse onto each other, once they are rescaled by ℓ . Here we are assuming that fermion parity is not conserved, which yields finite jumps in $I[\Delta\phi]$ at the level-crossing values of the phase difference, $\Delta\phi = \frac{\pi}{2} + k\pi$, k integer, by accordingly setting to π the period of $I[\Delta\phi]$; **b)** Same as in panel **a)**, but now assuming fermion parity conservation. There are accordingly no more jumps at $\Delta\phi = \frac{\pi}{2} + k\pi$ and the full periodicity of 2π in $\Delta\phi$ has been restored.

After dropping $[i\eta_1\eta_2]$, the boundary Hamiltonian, as well as the “bulk” Hamiltonian describing the chains, are both quadratic in the fermion operators; as a result, they can be exactly diagonalized and the spin current can be evaluated.

In Fig.2 we provide a sample of the results for the equilibrium spin current through the junction. To derive the current, we numerically perform the exact diagonalization of the real-space Hamiltonian. As a result, we find that $I_1 = -I_2$ and that, as expected, both currents only depend on the phase difference $\Delta\phi = \phi_1 - \phi_2$.

In computing the spin current, an important point to address is whether the total JW fermion parity (that is, the z -component of the total spin) is conserved, or not. To account for both possibilities, in Fig.2, we draw $I_1[\Delta\phi] \equiv I[\Delta\phi]$ as a function of $\Delta\phi$, computed, both by assuming that fermion parity is not conserved (Fig.2a), and by assuming that fermion parity is conserved (Fig.2b), for the values of the parameters reported in the figure caption. In drawing all the plots we have set $\tau = 1$. For $\tau = 1$ we recover pure-Andreev reflection at both boundaries as soon as $\ell \geq \frac{2\pi J^2 \sin(k_F)}{\tau^2} \sim 5$. Accordingly, to describe the results of Fig.2 we may safely rely on the field-theory approach developed in Appendix C by approximating the lattice fermion operator $c_{j,\lambda}$ at time t ($\lambda = 1, 2$) as

$$c_{j,\lambda}(t) \approx e^{-i\phi_\lambda} \{e^{ik_F j} \psi_\lambda(x_j - \ell - vt) - e^{-ik_F j} \psi_\lambda^\dagger(\ell - x_j - vt)\} \quad , \quad (18)$$

with $\psi_\lambda(x - vt)$ being chiral fermionic fields, $-2J \cos(k_F) - H = 0$, $v_F = 2J \sin(k_F)$ and with $x_j = aj$, a being the lattice step (which we set to 1 henceforth). Inserting Eq.(18) into Eq.(17) and getting rid, of the operator $[i\eta_1\eta_2]$, we reexpress $H_\Delta^{(2)}$ in terms of the continuum field operators as

$$H_\Delta^{(2)} \rightarrow iJ_\Delta \{e^{i\Delta\phi} [e^{-ik_F} \psi_1^\dagger(-\ell) - e^{ik_F} \psi_1(\ell)][e^{ik_F} \psi_2(-\ell) - e^{-ik_F} \psi_2^\dagger(\ell)] - \text{h.c.}\} \quad . \quad (19)$$

The operator at the right-hand side of Eq.(19) is bilinear in the local fermionic fields at $x = \pm\ell$, and it corresponds to a purely marginal perturbation, not inducing any scaling with ℓ in the

boundary operator itself. Therefore, we expect no additional scaling in $I[\Delta\phi]$, besides the one with ℓ^{-1} that characterizes the equilibrium supercurrent across a noninteracting fermionic system [46, 47, 33, 48, 49]. Apparently, this is fully consistent with the plots we draw in Fig.2 at different values of ℓ .

Regarding fermion parity conservation we note that, in a “fermionic” SNS junction, the conservation of the total fermion parity is expected to hold, especially in the absence of gapless, Fermi liquid-like, quasiparticle baths and/or in the presence of “fast” variations in time of the system parameters, which do not allow the system to relax toward the actual minimum energy state, at the cost of changing its total fermion parity. At variance, in a spin system, fermion parity corresponds to the total spin conservation along the z -axis, which can be readily broken by means of, e.g., impurities, local magnetic field fluctuations, etc.

The non conservation of fermion parity leads to the discontinuity in $I[\Delta\phi]$ at $\Delta\phi = \frac{\pi}{2} + k\pi$. To discuss this point, we rely on the formalism of Appendix C. In particular, considering the weak coupling limit $J_\Delta/J \ll 1$, we note that we may consistently assume that both chains terminate at $j = 1$ (open boundary conditions). The allowed energy eigenvalues in each chain are therefore determined by solving Eqs.(C.12) of Appendix C. These always take a zero-energy solution, with the Bogoliubov-de Gennes (BDG) wavefunction in chain- λ given by

$$\begin{bmatrix} u_{j;0;\lambda} \\ v_{j;0;\lambda} \end{bmatrix} = \frac{1}{\sqrt{2(\ell+1)}} \begin{bmatrix} ie^{-i\phi_\lambda} \sin(k_F j) \\ -ie^{i\phi_\lambda} \sin(k_F j) \end{bmatrix} . \quad (20)$$

The corresponding zero-mode operators, $\Gamma_{0;\lambda}$, are therefore given by

$$\Gamma_{0;\lambda} = \frac{e^{-i\phi_\lambda}}{\sqrt{2(\ell+1)}} \sum_{j=1}^{\ell} \{i \sin(k_F j) [c_{j,\lambda} - c_{j,\lambda}^\dagger]\} - \frac{2J e^{-i\phi_\lambda} \sin[k_F(\ell+1)]}{\tau \sqrt{2(\ell+1)}} \gamma_\lambda . \quad (21)$$

Aside from the over-all phase factor $e^{-i\phi_\lambda}$, $\Gamma_{0;\lambda}$ is a real fermion operator. When considering the two (still disconnected) chains all together, the two real zero-modes $\Gamma_{0;1}$ and $\Gamma_{0;2}$, can be combined into a complex fermionic zero-mode operator $a_0 = \frac{1}{2} \{\Gamma_{0;1} + i\Gamma_{0;2}\}$. In the disconnected limit, the $N = 2$ -junction spectrum is twofold degenerate, with the two degenerate states (for each energy eigenvalue) corresponding to the mode a_0 being empty, or full (that is, with different JW fermion parity). On turning on the interaction, a finite hybridization between the zero-mode operators at the two chains sets in, with a strength proportional to J_Δ and modulated by $\Delta\phi$. In fact, this can be readily inferred from Eq.(19) by truncating the mode decomposition of the fermion field operators to the zero-modes, thus getting the “restricted” Hamiltonian involving the zero-mode operators, given by

$$H_{\Delta;0}^{(2)} = \frac{4i \sin^2(k_F) J_\Delta \cos(\Delta\phi)}{\ell+1} \Gamma_{0;1} \Gamma_{0;2} = \frac{4 \sin^2(k_F) J_\Delta \cos(\Delta\phi)}{\ell+1} \{2a_0^\dagger a_0 - 1\} . \quad (22)$$

From Eq.(22) we see that, for $0 \leq \Delta\phi < \frac{\pi}{2}$, the actual groundstate corresponds to having the a_0 -mode empty. At variance, for $\frac{\pi}{2} < \Delta\phi \leq \pi$, the groundstate corresponds to the a_0 -mode filled by one JW fermion, with opposite fermion parity. If fermion parity is not conserved, then the level crossing at $\Delta\phi = \frac{\pi}{2}$ implies a finite discontinuity in $I[\Delta\phi]$, which is the feature evidenced in the

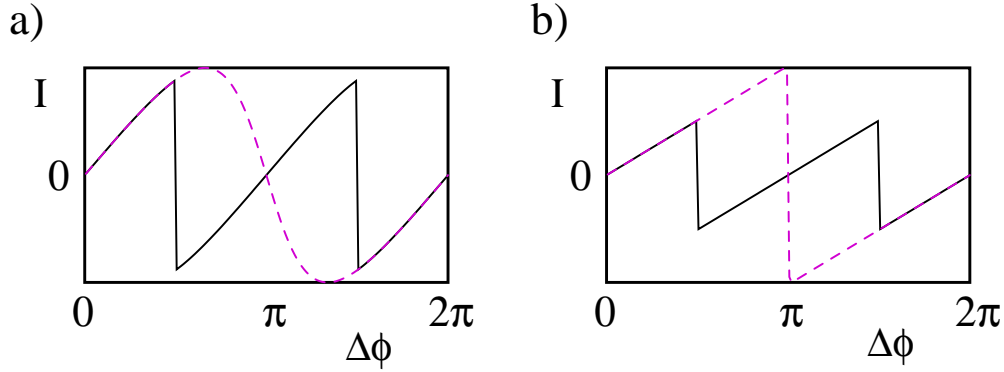


Figure 3: **a)** $I[\Delta\phi]$ as a function of $\Delta\phi$ through an $N = 2$ -junction with $J = 1$ computed by exact diagonalization with $\tau = 1$, $\mu = 0.05$, $\ell = 100$, and $J_\Delta = 0.4$ in the case in fermion parity is not preserved (black full curve), as well as in the case in which it is preserved (dashed magenta curve); **b)** Same as in panel **a)**, but with $J_\Delta = 1.0$.

plots of Fig.2a). At variance, if fermion parity is conserved, the finite jump is substituted by a smooth, continuous curve, determined by the impossibility for the system to undergo the switch toward the “true” groundstate at $\Delta\phi = \frac{\pi}{2}$ without changing the total fermion parity, as it appears in Fig.2b) [51, 22, 48].

An additional comment is in order to deal with the periodicity of $I[\Delta\phi]$ as a function of $\Delta\phi$ both in the case in which the fermion parity \mathcal{P} is not conserved, as well as in the case in which it is conserved. In the former case, $I[\Delta\phi]$ is periodic with period equal to π , that is, to the minimal interval of values of $\Delta\phi$ separating two consecutive level crossings as described by Eq.(22) (see also the analysis of Appendix B for a comprehensive discussion of this point). In the latter case, the periodicity is restored back to 2π , as we display in Fig.3, where we draw a synoptic plot of $I[\Delta\phi]$ for the same values of the system parameters and of ℓ , but computed with, and without, assuming that \mathcal{P} is conserved. The two periodicities are halved, with respect to what we expect to get in the case of a fermionic quantum wire between two topological superconductors at fixed phase difference, which is expected, as a consequence of the JW transformation applied to the quantum spin chain [43].

Finally, while, as $H_\Delta^{(2)}$ is a truly marginal interaction, with no induced running of the coupling strengths, tuning “by hand” J_Δ/J , it is still possible to trigger a crossover between the sinusoidal dependence of $I[\Delta\phi]$ on $\Delta\phi$, which is typical of the weakly coupled regime $J_\Delta/J \ll 1$, and the sawtooth one, which takes place when $J_\Delta \sim J$ [52, 33]. To address this (non-dynamically induced) crossover in $I[\Delta\phi]$, in Fig.4 we draw $I[\Delta\phi]$ as a function of $\Delta\phi$ for the same values of the parameters as we used to draw Fig.2; we consider both cases in which the fermion parity is not conserved (Fig.4a)), and is conserved (Fig.4b)). We set $\ell = 100$ and vary J_Δ/J , as discussed in the caption. The crossover from the sinusoidal to the sawtooth behavior is apparent, whether \mathcal{P} is conserved, or not.

We now move to discussing the $N = 3$ junction, in which the KFs are expected to play a crucial role in determining the emergence of the topological Kondo effect [36, 37, 39].

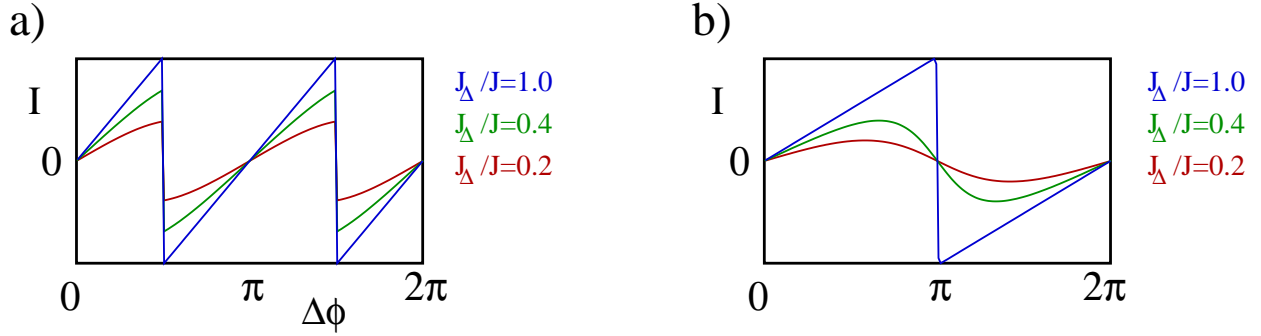


Figure 4: **a)** $I[\Delta\phi]$ as a function of $\Delta\phi$ through an $N = 2$ -junction with $J = 1$ computed by exact diagonalization by assuming that fermion parity is not conserved, with $\tau = 1$, $\mu = 0.05$, $\ell = 100$, and $J_\Delta = 1.0$ (blue curve), $J_\Delta = 0.4$ (green curve), $J_\Delta = 0.2$ (red curve); **b)**: The same as in panel **a)**, but now by assuming that fermion parity is conserved. The crossover from a sinusoidal to a sawtooth-like dependence of $I[\Delta\phi]$ on $\Delta\phi$ on increasing J_Δ/J is apparent.

4. Effective Hamiltonian and groundstate structure of the $N = 3$ -junction

Differently from the $N = 2$ -junction, the $N = 3$ -junction is not exactly solvable, due to the nontrivial effect of the KFs $\{\eta_\lambda\}$ on the boundary interaction. Indeed, in this case the KFs combine into an effective impurity spin-1/2 degree of freedom, thus determining a peculiar realization of the TKE at our junction. The TKE emerges in our system just as at a junction of three quantum Ising chains [37, 38], or of three XX chains [36], of three one-dimensional Josephson junction arrays [34], and of three XY chains [39]. For this reason, we attack the problem by means of the standard RG approach to a boundary impurity model, within the field theory framework developed in Appendix [Appendix C](#).

In terms of the continuum fermionic fields, the junction Hamiltonian, $H_\Delta^{(3)}$, is given by

$$H_\Delta^{(3)} = J_\Delta \sum_{\lambda=1}^3 \{e^{i[\phi_\lambda - \phi_{\lambda+1}]} [i\eta_\lambda \eta_{\lambda+1}] i[e^{-ik_F} \psi_\lambda^\dagger(-\ell) - e^{ik_F} \psi_\lambda(\ell)] [e^{ik_F} \psi_{\lambda+1}(-\ell) - e^{-ik_F} \psi_{\lambda+1}^\dagger(\ell)] + \text{h.c.}\}, \quad (23)$$

with $\lambda + 3 \equiv \lambda$.

The key feature of $H_\Delta^{(3)}$ in Eq.(23) is the explicit dependence of the Kondo interaction on the phase differences $\phi_\lambda - \phi_{\lambda+1}$. This induces a dependence on the applied phases in the groundstate energy of our system. Thus, when differentiating the groundstate energy with respect to the applied phases, one has a nonzero equilibrium spin current pattern through the junction. Monitoring the spin current at different scales provides an effective tool to map out the phase diagram of the system.

The idea of probing the phase diagram of junctions of one-dimensional systems by measuring the equilibrium current pattern through the system has been largely exploited in the literature regarding junctions of one-dimensional Josephson junction arrays [33, 41, 34, 42, 53]. Here, we show how our approach extends this technique to junctions of quantum spin chains, by means of a pertinent generalization of the methods developed in Ref.[43] for a single spin chain.

In the weak coupling limit, $J_\Delta/J \ll 1$, we assume open boundary conditions for the lattice

fields $c_{j,\lambda}$ at the inner boundary, that is, $c_{j=0,\lambda} = 0, \forall \lambda$. As a result, Eq.(23) becomes

$$H_{\Delta}^{(3)} = 4 \sum_{\lambda=1}^3 J_{\lambda,\lambda+1} \sin^2(k_F) [i\eta_{\lambda}\eta_{\lambda+1}][i\xi_{\lambda}(0)\xi_{\lambda+1}(0)] \quad , \quad (24)$$

with $\xi_{\lambda}(x)$ being chiral real fermionic fields and $J_{\lambda,\lambda+1} = J_{\Delta} \cos[\phi_{\lambda} - \phi_{\lambda+1}]$. $H_{\Delta}^{(3)}$ in Eq.(24) corresponds to the (in general anisotropic) Kondo interaction arising at a junction of three quantum Ising chains [37, 39]. The anisotropy is determined by the phase differences and, for large enough values of the phase differences, the interaction strengths can even take different signs.

To set up the field theory approach to the interacting boundary problem defined by $H_{\Delta}^{(3)}$ in Eq.(24), we have to first construct the system's groundstate by pertinently taking into account the emerging real-fermion zero-mode operators $\Gamma_{0;\lambda}$, as well as the possible degeneracy associated to different eigenvalues of the total fermion parity operator. To do so, we single out the zero-mode contribution to the mode expansion of the ξ_{λ} fields at the right-hand side of Eq.(24), by writing the corresponding contribution to $H_{\Delta}^{(3)}$, $H_{\Delta;0}^{(3)}$, as

$$H_{\Delta;0}^{(3)} = 4 \sum_{\lambda=1}^3 \frac{J_{\lambda,\lambda+1} \sin^2(k_F)}{\ell + 1} [i\eta_{\lambda}\eta_{\lambda+1}][i\Gamma_{0;\lambda}\Gamma_{0;\lambda+1}] \quad . \quad (25)$$

$H_{\Delta;0}^{(3)}$ in Eq.(25) describes a dipole interaction between two effective spin-1/2 spin operators. A key point is that, naively rewriting it down as $H_{\Delta;0}^{(3)} \rightarrow \sum_{\lambda=1}^3 G_{\lambda} \sigma_{\eta}^{\lambda} \sigma_{\Gamma}^{\lambda}$, with σ_{η}^{λ} and $\sigma_{\Gamma}^{\lambda}$ being Pauli matrices acting over orthogonal spaces and G_{λ} being pertinently defined constants, would lead to an incorrect state counting (6 independent real Majorana modes would correspond to 3 pairs of complex Dirac modes, together with their Hermitean conjugate, which would yield a total of 8 independent states. At variance, the construction with the Pauli matrices would imply a total of 4 independent states). In fact, the correct way of realizing the fermion operators entering $H_{\Delta;0}^{(3)}$ is provided by a straightforward generalization of the Lee-Wilczek construction [54], which we reformulate and adapt to our model in Appendix Appendix D.

In order to properly diagonalize $H_{\Delta;0}^{(3)}$ in Eq.(25), following the derivation of Appendix Appendix D, we define the state $|a_{\Gamma}, a_{\eta}\rangle_{\gamma}$ so that

$$\begin{aligned} \sigma_{\Gamma}^3 |a_{\Gamma}, a_{\eta}\rangle_{\gamma} &= [i\Gamma_{0;1}\Gamma_{0;2}] |a_{\Gamma}, a_{\eta}\rangle_{\gamma} = a_{\Gamma} |a_{\Gamma}, a_{\eta}\rangle_{\gamma} \\ \sigma_{\eta}^3 |a_{\Gamma}, a_{\eta}\rangle_{\gamma} &= [i\eta^1 \eta^2] |a_{\Gamma}, a_{\eta}\rangle_{\gamma} = a_{\eta} |a_{\Gamma}, a_{\eta}\rangle_{\gamma} \\ \mathcal{P}_{\tau} |a_{\Gamma}, a_{\eta}\rangle_{\gamma} &= \gamma |a_{\Gamma}, a_{\eta}\rangle_{\gamma} \quad , \end{aligned} \quad (26)$$

with $\mathcal{P}_{\tau} = P_{\Gamma} \cdot P_{\eta}$, P_{Γ} being the fermion parity associated to the triple $\{\Gamma_{0;1}, \Gamma_{0;2}, \Gamma_{0;3}\}$, P_{η} being the fermion parity associated to the triple $\{\eta^1, \eta^2, \eta^3\}$, and $a_{\Gamma}, a_{\eta}, \gamma = \pm 1$. In addition, consistently with the mode expansion of Eq.(C.14) of Appendix Appendix C, we set $\xi_{n,\lambda} |a_{\Gamma}, a_{\eta}\rangle_{\gamma} = 0, \forall n > 0$ and $\forall a_{\Gamma}, a_{\eta}, \gamma, \lambda$. As we show in Eqs.(D.13), what is the actual groundstate of $H_{\Delta;0}^{(3)}$ (plus the bulk Hamiltonian in the disconnected junction limit) depends on the relative values of the coupling strengths $J_{\lambda,\lambda+1}$ and, in particular, on their sign. Expressing $J_{\lambda,\lambda+1}$ in terms of the independent phase differences $\Delta\phi_a = \phi_1 - \phi_2$ and $\Delta\phi_b = \phi_1 - \phi_3$, from Eqs.(D.13) we obtain that the groundstate has energy $\mathcal{E}_3^{(0)}[\Delta\phi_a, \Delta\phi_b]$, given by

$$\mathcal{E}_3^{(0)}[\Delta\phi_a, \Delta\phi_b] = -\frac{4J_\Delta \sin^2(k_F)}{\ell + 1} \times \max_{\lambda_a, \lambda_b = \pm 1} \{ \lambda_a \cos(\Delta\phi_a) + \lambda_b \cos(\Delta\phi_b) + \lambda_a \lambda_b \cos(\Delta\phi_a - \Delta\phi_b) \} . \quad (27)$$

From the discussion above, we conclude that there are two states, corresponding to different values of γ , that minimize the energy, for each choice of λ_a and λ_b . Therefore, whether, on varying $\Delta\phi_a$ and/or $\Delta\phi_b$, at a level crossing for the groundstate, the system remains within the initial states or “jumps” into the actual groundstate, is not a matter of whether the fermion parity is conserved, or not, but rather of whether the system is allowed to crossover from, e.g., the singlet state at the first line of Eq.(D.13) to the triplet state at the last line of the same equation. In the latter case, the equilibrium spin currents within each one of the three chains, $I_1[\Delta\phi_a, \Delta\phi_b]$, $I_2[\Delta\phi_a, \Delta\phi_b]$, $I_3[\Delta\phi_a, \Delta\phi_b]$ are respectively given by (to leading order in J_Δ)

$$\begin{aligned} I_1[\Delta\phi_a, \Delta\phi_b] &= \frac{\partial \mathcal{E}_3^{(0)}[\Delta\phi_a, \Delta\phi_b]}{\partial \Delta\phi_a} + \frac{\partial \mathcal{E}_3^{(0)}[\Delta\phi_a, \Delta\phi_b]}{\partial \Delta\phi_b} = \frac{4J_\Delta \sin^2(k_F)}{\ell + 1} [\lambda_a \sin(\Delta\phi_a) + \lambda_b \sin(\Delta\phi_b)] \\ I_2[\Delta\phi_a, \Delta\phi_b] &= -\frac{\partial \mathcal{E}_3^{(0)}[\Delta\phi_a, \Delta\phi_b]}{\partial \Delta\phi_a} = -\frac{4J_\Delta \sin^2(k_F)}{\ell + 1} [\lambda_a \sin(\Delta\phi_a) + \lambda_a \lambda_b \sin(\Delta\phi_a - \Delta\phi_b)] \\ I_3[\Delta\phi_a, \Delta\phi_b] &= -\frac{\partial \mathcal{E}_3^{(0)}[\Delta\phi_a, \Delta\phi_b]}{\partial \Delta\phi_b} = -\frac{4J_\Delta \sin^2(k_F)}{\ell + 1} [\lambda_b \sin(\Delta\phi_b) - \lambda_a \lambda_b \sin(\Delta\phi_a - \Delta\phi_b)] . \quad (28) \end{aligned}$$

In the former case, instead, the currents are determined by just the initial state of the system, which sets once, and forever, the values of λ_a and λ_b , regardless of $\Delta\phi_a$ and $\Delta\phi_b$. In a real life experiment, fluctuations, local fields, impurities, as well as Landau-Zener like transitions induced by nonadiabatic changes in the applied phases [55], are likely to favor the scenario described by Eqs.(28). Yet, for the sake of completeness, in the following we keep discussing both scenarios, when possible. As a main remark, it is worth pointing out that, for any choice of λ_a, λ_b (and, therefore, both when the system keeps within its true ground state, or it does not), the currents in Eqs.(28) are consistent with “Kirchoff law” at the junction, $\sum_{\lambda=1}^3 I_\lambda[\Delta\phi_a, \Delta\phi_b] = 0$.

We note that the current pattern in Eqs.(28) might look like what one would expect at a junction between three spinless normal conducting wires connected to three topological superconductors at fixed phases of the superconducting leads. However, in this latter case, changing ℓ would simply result in a rescaling of $I_\lambda[\Delta\phi_a, \Delta\phi_b]$ with ℓ^{-1} . Eventually, including the effects of the dynamical, finite-energy bulk modes of the wires would just provide a slight change in the functional dependence of the currents on $\Delta\phi_a, \Delta\phi_b$, without affecting the scaling with ℓ^{-1} . Instead, as we discuss in the following, in a junction between spin chains, TKE does affect the scaling properties of the currents, as ℓ becomes of the order of ℓ_K .

To provide a synoptic view of the changes in the groundstate of the system as functions of the applied phases, in Fig.5 we report the regions in the $\Delta\phi_a - \Delta\phi_b$ -plane corresponding to different values of λ_a, λ_b . Assuming that the current pattern through the junction is always determined by the “actual” groundstate of the system, Fig.5 also provides a synoptic view of how the branches of the currents in Eqs.(28) vary depending on the applied phase differences $\Delta\phi_a, \Delta\phi_b$.

We now resort to the RG approach, to discuss the nonperturbative effects that arise when $\ell \sim \ell_K$.

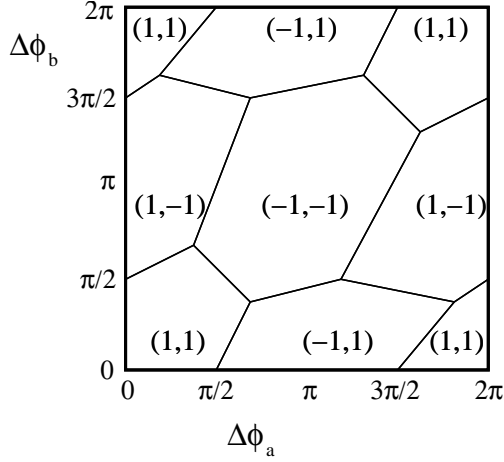


Figure 5: Regions in the $\Delta\phi_a - \Delta\phi_b$ plane in which the current pattern through the $N = 3$ -junction is determined by Eqs.(28) with the values of $(\lambda_a, \lambda_b) = (\pm 1, \pm 1)$ reported in the figure. Due to the periodicity of the currents in both $\Delta\phi_a$ and $\Delta\phi_b$, we limit the plot to the square $0 \leq \Delta\phi_a, \Delta\phi_b \leq 2\pi$. If the system keeps within its actual groundstate when crossing a borderline between different regions, the currents are expected to exhibit finite discontinuities at the crossings, similar to what happens to $I[\Delta\phi]$ in the $N = 2$ junction at $\Delta\phi = \frac{\pi}{2}$.

5. Renormalization group approach to the topological Kondo effect at the $N = 3$ junction

To implement the RG approach, we resort to the imaginary time framework and describe the boundary interaction in terms of the imaginary time action $S_{\Delta}^{(3)} = \int_0^{\beta} d\tau H_{\Delta}^{(3)}(\tau)$, with $H_{\Delta}^{(3)}(\tau)$ being the boundary action in the interaction representation at imaginary time τ and $\beta = (k_B T)^{-1}$. To carefully take into account the role of the zero-mode operators, we write the operator $\xi_{\lambda}(0)$ at imaginary time τ , $\xi_{\lambda}(\tau)$, as

$$\xi_{\lambda}(\tau) = \frac{\Gamma_{0;\lambda}}{\sqrt{\ell+1}} + \bar{\xi}_{\lambda}(\tau) \quad . \quad (29)$$

From Eq.(29) we obtain $S_{\Delta}^{(3)} = S_{\Delta;1}^{(3)} + S_{\Delta;2}^{(3)} + S_{\Delta;3}^{(3)}$, with

$$\begin{aligned} S_{\Delta;1}^{(3)} &= \frac{4 \sin^2(k_F)}{\ell+1} \sum_{\lambda=1}^3 J_{\lambda,\lambda+1} \int_0^{\beta} d\tau [i\eta_{\lambda}(\tau)\eta_{\lambda+1}(\tau)] [i\Gamma_{0;\lambda}(\tau)\Gamma_{0;\lambda+1}(\tau)] \\ S_{\Delta;2}^{(3)} &= \frac{4 \sin^2(k_F)}{\sqrt{\ell+1}} \sum_{\lambda=1}^3 J_{\lambda,\lambda+1} \int_0^{\beta} d\tau [i\eta_{\lambda}(\tau)\eta_{\lambda+1}(\tau)] i\{\Gamma_{0;\lambda}(\tau)\bar{\xi}_{\lambda+1}(\tau) + \bar{\xi}_{\lambda}(\tau)\Gamma_{0;\lambda+1}(\tau)\} \\ S_{\Delta;3}^{(3)} &= 4 \sin^2(k_F) \sum_{\lambda=1}^3 J_{\lambda,\lambda+1} \int_0^{\beta} d\tau [i\eta_{\lambda}(\tau)\eta_{\lambda+1}(\tau)] [i\bar{\xi}_{\lambda}(\tau)\bar{\xi}_{\lambda+1}(\tau)] \quad . \end{aligned} \quad (30)$$

Out of the three contributions in Eqs.(30), $S_{\Delta;1}^{(3)}$ is exactly accounted for by diagonalizing $H_{\Delta;0}^{(3)}$ and by determining the groundstate accordingly. The interaction between the zero-modes and the dynamical modes of the ξ_{λ} fields, as well as the interaction between the dynamical modes

themselves, provides a nontrivial renormalization to the $J_{\lambda,\lambda+1}$ and, therefore, to the groundstate energy.

To explicitly derive the corresponding RG equations, we introduce a high-energy cutoff $D_0 \sim 2J$ and then we progressively reduce D_0 to $D = D_0 - \delta D$, by integrating over the modes lying in the energy windows between $-D_0$ and $-D_0 + \delta D$ and $D_0 - \delta D$ and D_0 . To do so, we write down the partition function \mathcal{Z} as

$$\mathcal{Z} = \mathcal{Z}_0 \langle \mathbf{T}_\tau e^{-S_{\Delta;l}^{(3)}} \rangle_0, \quad (31)$$

with $\langle \dots \rangle_0$ denoting averaging over the bulk action at disconnected junction plus $S_{\Delta;1}^{(3)}$, $S_{\Delta;l}^{(3)} = S_{\Delta;2}^{(3)} + S_{\Delta;3}^{(3)}$ and \mathcal{Z}_0 being the partition function of the ‘‘unperturbed’’ system (with only $S_{\Delta;1}^{(3)}$ as a nonzero boundary action).

Expanding \mathcal{Z} up to second-order in the $J_{\lambda,\lambda+1}$, we have to perform the contractions leading to the terms that renormalize $S_{\Delta;1}^{(3)}$. In doing so, we have to pay particular attention to the correlation function of the Klein factors, ${}_\gamma \langle \psi_1 | \eta^\lambda(\tau_1) \eta^\lambda(\tau_2) | \psi_1 \rangle_\gamma$. Specifically, using Lehman’s representation for the correlation function in combination with the results of Appendix [Appendix D](#) and assuming that $|\psi_1\rangle_\gamma$ is the groundstate of the junction, we obtain

$${}_\gamma \langle \psi_1 | \eta^\lambda(\tau_1) \eta^\lambda(\tau_2) | \psi_1 \rangle_\gamma = e^{-\left[\frac{8 \sin^2(k_F) J_{\lambda+1, \lambda+2}}{\ell+1} \right] (\tau_1 - \tau_2)}. \quad (32)$$

In addition, we need the finite-temperature, imaginary time ordered correlation function of the dynamical modes, which is given by

$$\langle \mathbf{T}_\tau \bar{\xi}_\lambda(\tau) \bar{\xi}_{\lambda'}(\tau') \rangle = -\frac{2\delta_{\lambda,\lambda'}}{\frac{\beta}{\pi} \sin \left[\frac{\pi}{\beta} (\tau - \tau') \right]}. \quad (33)$$

Using the result of Eq.(32,33), introducing the short-imaginary-time distance cutoff τ_c and rescaling τ_c to $\tau_c + \delta\tau_c$, we find that $S_{\Delta;1}^{(3)}$ is corrected by a term $\delta S_{\Delta;1}^{(3)}$ given by

$$\delta S_{\Delta;1}^{(3)} = -\frac{4[4 \sin^2(k_F)]^2 \delta\tau_c}{\tau_c(\ell+1)} \sum_{\lambda=1}^3 J_{\lambda,\lambda+1} J_{\lambda+1,\lambda+2} \int_0^\beta d\tau e^{-\left[\frac{8 \sin^2(k_F) J_{\lambda+1, \lambda+2} \tau_c}{\ell+1} \right]} [i\eta_{\lambda+2}(\tau) \eta_\lambda(\tau)] [i\Gamma_{0,\lambda+2}(\tau) \Gamma_{0,\lambda}(\tau)]. \quad (34)$$

From Eq.(34), we eventually infer the RG equations for the running couplings by looking at how the cutoff-dependent corrections vary as a function of the cutoff itself. As a result, defining the dimensionless running couplings $G_{\lambda,\lambda+1}$ as

$$G_{\lambda,\lambda+1} = \frac{4 \sin^2(k_F) J_{\lambda,\lambda+1}}{v} = 2 \sin(k_F) \frac{J_{\lambda,\lambda+1}}{J}, \quad (35)$$

we obtain the RG equations for the running couplings, given by

$$\begin{aligned} \frac{dG_{1,2}}{dl} &= e^{-\frac{2|G_{1,2}|}{\ell+1}} G_{2,3} G_{3,1} \equiv \hat{\beta}_{1,2}[\{G_{\lambda,\lambda+1}\}] \\ \frac{dG_{2,3}}{dl} &= e^{-\frac{2|G_{2,3}|}{\ell+1}} G_{3,1} G_{1,2} \equiv \hat{\beta}_{2,3}[\{G_{\lambda,\lambda+1}\}] \\ \frac{dG_{3,1}}{dl} &= e^{-\frac{2|G_{3,1}|}{\ell+1}} G_{1,2} G_{2,3} \equiv \hat{\beta}_{3,1}[\{G_{\lambda,\lambda+1}\}] \quad , \end{aligned} \quad (36)$$

with $l = \ln\left(\frac{D_0}{D}\right)$, and $D \sim \pi v/\ell$ being the running energy scale. Note that, in writing Eqs.(36), we have set $\tau_c = a/v$, with a being the lattice step. Importantly, we note that the same equations arise when deriving the renormalization of the coupling strengths in $S_{\Delta;3}^{(3)}$ to second order in the $J_{\lambda,\lambda+1}$. Also, as we have introduced the absolute values of the running couplings at the exponents of the right-hand side of Eqs.(36), they hold regardless the system groundstate corresponds to $|\psi_1\rangle_\gamma$, or to any other of the states listed in Eqs.(D.13).

An important observation is that, as long as $|G_{\lambda,\lambda+1}(D)|/(\ell + 1) \ll 1$, we may neglect the exponential factors at the right-hand side of Eqs.(36), so that they reduce to

$$\begin{aligned}\frac{dG_{1,2}}{dl} &= G_{2,3}G_{3,1} \equiv \beta_{1,2}[\{G_{\lambda,\lambda+1}\}] \\ \frac{dG_{2,3}}{dl} &= G_{3,1}G_{1,2} \equiv \beta_{2,3}[\{G_{\lambda,\lambda+1}\}] \\ \frac{dG_{3,1}}{dl} &= G_{1,2}G_{2,3} \equiv \beta_{3,1}[\{G_{\lambda,\lambda+1}\}] \quad .\end{aligned}\tag{37}$$

Eqs.(37) are the standard RG equations for the topological Kondo effect [37]. In appendix [Appendix E](#) we discuss in detail the general features of the solutions of Eqs.(37) for the various possible sign assignment of the bare couplings. Here, we focus onto the specific consequences of Eqs.(37) for our junction.

As a first observation, we note that, except for some specific lines in parameter space (see the next Section and Appendix [Appendix E](#) for details), Eqs.(37) always imply a flow toward the Kondo fixed point. In particular, to double-check the validity of the approximation leading to Eqs.(37), we note that the energy splitting between the groundstate of $H_{\Delta;0}^{(3)}$ and its first excited state is of order of $\bar{\epsilon}_G = 8|J_{\lambda,\lambda+1}|\sin^2(k_F)/(\ell + 1)$, while the energy required to excite a ‘‘dynamical’’ mode of $\bar{\xi}_\lambda(\tau)$ is, instead, as large as $\delta\epsilon = \pi v/(\ell + 1) = 2\pi J \sin(k_F)/(\ell + 1)$. As a result, we find that $\bar{\epsilon}_G/\delta\epsilon \sim |G_{\lambda,\lambda+1}|/\pi$. Accordingly, as long as $|G_{\lambda,\lambda+1}| \ll 1$ (that is, within the perturbative regime), finite-energy, dynamical modes of ξ_λ lie pretty higher in energy than the excited states of $H_{\Delta;0}^{(3)}$. This enables us to derive the spin currents just as we have done in Sec.4, by simply substituting the bare Kondo couplings with the renormalized (running) ones.

The running couplings depend on $\Delta\phi_a, \Delta\phi_b$ via their initial values $G_{\lambda,\lambda+1}^{(0)}$. Thus, it is in principle straightforward to derive the spin current pattern from the integral curves of Eqs.(36) by just differentiating with respect to the phase differences. This picture breaks down at the scale \tilde{D} at which $|G_{\lambda,\lambda+1}(\tilde{D})| \sim 1$. This condition is a signal of the onset of the nonperturbative regime and, accordingly, we identify \tilde{D} with D_K . As a result, we conclude that the (improved) formula expressing the spin current pattern across the junction in terms of derivatives of the running couplings with respect to the phase differences holds all the way down to $D \sim D_K$.

To infer the behavior of the junction near the strongly coupled Kondo fixed point, we note that, as we point out in Appendix [Appendix E](#), the anisotropy between the (absolute values of the) boundary couplings is in general suppressed along the RG trajectories. For this reason, we tentatively construct the effective boundary Hamiltonian at the strongly coupled Kondo fixed point by pertinently adapting the derivation done in Ref.[39] in the isotropic case. Specifically, our Kondo Hamiltonian corresponds to the realization of the two-channel spin-1/2 Kondo model discussed in Refs.[56, 57]. At the fixed point, this exhibits a remarkable ‘‘fractional degeneracy’’

[58, 59, 7, 60, 6], which is encoded in the emergence of two energy degenerate total spin singlet groundstates at the strongly coupled fixed point, $|\Sigma\rangle_1, |\Sigma\rangle_2$ [56, 57, 39].

As discussed above, the isotropic fixed point is expected to faithfully describe also the strongly coupled regime for boundary couplings different from each other. Since the differences in the boundary couplings are directly related to their dependence on the applied phases, we readily conclude that all the spin currents through the junction must be equal to zero at the Kondo fixed point. In order to build the leading boundary operator at the strongly coupled fixed point, we assume that close to, but not exactly at, the Kondo fixed point, the coupling strengths keep (slightly) different from each other. Therefore, we repeat the construction of Appendix A of Ref.[39], getting, as final result, the boundary perturbation that, in terms of the lattice fields $\{c_{j,\lambda}\}$, is given by

$$H_{\Delta;\text{Sc}}^{(3)} = i\mathbf{V}^y \left\{ \sum_{\lambda=1}^3 \frac{3J^3}{[J_{\lambda+1,\lambda+2} + J_{\lambda+2,\lambda}]^2} \right\} \prod_{\lambda=1}^3 [c_{2,\lambda}^\dagger + c_{2,\lambda}] \quad , \quad (38)$$

with \mathbf{V}^y acting on the degenerate singlets as $\mathbf{V}^y|\Sigma\rangle_{1,2} = \mp i|\Sigma\rangle_{2,1}$, and the operators $\{c_{1,\lambda}, c_{1,\lambda}^\dagger\}$ hybridized with the topological spin determined by the Klein factors into either one of the degenerate singlets [56, 39]. Since the lattice field operators at $j = 1$ are hybridized with the topological spin operator, in order to resort to the analog of the low-energy, long-wavelength expansion in Eq.(C.8), we have to impose open boundary conditions on the lattice fields at $j = 2$. Once the boundary conditions corresponding to perfect Andreev reflection at the outer boundaries are accounted for, as well, Eq.(38) yields, in the continuum field theory framework

$$H_{\Delta;\text{Sc}}^{(3)} \rightarrow i\mathbf{V}^y \left\{ \sum_{\lambda=1}^3 \frac{3[\sin(k_F)J]^3}{[J_{\lambda+1,\lambda+2} + J_{\lambda+2,\lambda}]^2} \right\} \prod_{\lambda=1}^3 \xi_\lambda(0) \quad . \quad (39)$$

The operator at the right-hand side of Eq.(39) has scaling dimension $d = \frac{3}{2}$. It is, therefore, a strongly irrelevant operator in the infrared. Thus, its effects, including a possible nonzero contribution to the spin currents, are expected to vanish as we let the system flow to the Kondo fixed point. In fact, in order to evaluate such a contribution, we should know the specific dependence of the $J_{\lambda,\lambda+1}$ on $\Delta\phi_a, \Delta\phi_b$ in the strongly coupled regime. In principle, this could be derived by, e.g., employing techniques such as the ones developed in Refs.[61, 19]. However, this lies outside of the scope of this work, as we eventually show how the peculiar scaling properties of the spin current pattern through the junction at the onset of the nonperturbative Kondo regime provide an effective way of monitoring the emergence of the topological Kondo effect at our $N = 3$ junction of quantum spin chains.

In the following, we provide a guideline about how to do so by discussing a few, simple, paradigmatic cases of interest.

6. Spin current pattern at the onset of the Kondo regime

We explicitly solve Eqs.(37) in Appendix Appendix E where we show that, for generic values of the $G_{\lambda,\lambda+1}^{(0)}$, the solution is expressed in terms of the incomplete elliptic integral in Eq.(E.3). At the same time, we show how the solution is remarkably simplified if two of the three bare

couplings are equal to each other, say $G_{\lambda+1,\lambda+2}^{(0)} = G_{\lambda+2,\lambda}^{(0)}$. In this case, since $G_{\lambda+1,\lambda+2}^2(l) - G_{\lambda+2,\lambda}^2(l)$ is constant along the RG trajectories, we find that $G_{\lambda+1,\lambda+2}(l) = G_{\lambda+2,\lambda}(l)$ at any scale l . This extra constraint allows for providing explicit, closed-form formulas for the solution of Eqs.(37), which we discuss in detail in Appendix [Appendix E](#). Using those solutions with appropriate values for the initial boundary couplings $G_{\lambda,\lambda+1}^{(0)}$, in the following we explicitly derive the scaling of the spin currents for $\ell \leq \ell_K$ in two paradigmatic cases.

The first case corresponds to setting $\phi_1 = \phi_2 \neq \phi_3$, which implies $\Delta\phi_a = 0, \Delta\phi_b = \phi_1 - \phi_3 \neq 0$. In this case, we obtain

$$G_{1,2}^{(0)} = G_\Delta \quad , \quad G_{2,3}^{(0)} = G_{3,1}^{(0)} = G_\Delta \cos(\Delta\phi_b) \quad , \quad (40)$$

with $G_\Delta = \frac{4\sin^2(k_F)J_\Delta}{v}$. Accordingly, Eqs.(37) reduce to a set of two differential equations, given by

$$\begin{aligned} \frac{dG_{1,2}}{dl} &= G_{2,3}^2 \\ \frac{dG_{2,3}}{dl} &= G_{1,2}G_{2,3} \quad . \end{aligned} \quad (41)$$

Solving Eqs.(41) by using, as a running parameter, $l = \ln\left(\frac{\ell}{\ell_0}\right)$, with ℓ being the chain length and ℓ_0 a reference scale, we obtain

$$\begin{aligned} G_{1,2} \left[l = \ln\left(\frac{\ell}{\ell_0}\right) \right] &= G_\Delta \sin(\Delta\phi_b) \left\{ \frac{1 + \sin(\Delta\phi_b) + [1 - \sin(\Delta\phi_b)] \left(\frac{\ell}{\ell_0}\right)^{2G_\Delta \sin(\Delta\phi_b)}}{1 + \sin(\Delta\phi_b) - [1 - \sin(\Delta\phi_b)] \left(\frac{\ell}{\ell_0}\right)^{2G_\Delta \sin(\Delta\phi_b)}} \right\} \\ G_{2,3} \left[l = \ln\left(\frac{\ell}{\ell_0}\right) \right] &= G_\Delta \sin(\Delta\phi_b) \left\{ \frac{2 \cos(\Delta\phi_b) \left(\frac{\ell}{\ell_0}\right)^{G_\Delta \sin(\Delta\phi_b)}}{1 + \sin(\Delta\phi_b) - [1 - \sin(\Delta\phi_b)] \left(\frac{\ell}{\ell_0}\right)^{2G_\Delta \sin(\Delta\phi_b)}} \right\} \quad . \end{aligned} \quad (42)$$

Apparently, Eqs.(42) imply that, at any value of $\Delta\phi_b \neq \frac{\pi}{2} + k\pi$, with k integer, either all three the running couplings are > 0 , or two of them are < 0 , the third being > 0 . As we discuss in Appendix [Appendix E](#), this implies a flow towards the Kondo fixed point in both cases. This is evidenced by the explicit solutions at the right-hand side of Eqs.(42), which let us identify the $\Delta\phi_b$ -dependent Kondo length $\ell_K[\Delta\phi_b]$ given by

$$\ell_K[\Delta\phi_b] = \ell_0 \left\{ \frac{1 + |\sin(\Delta\phi_b)|}{1 - |\sin(\Delta\phi_b)|} \right\}^{\frac{1}{2G_\Delta |\sin(\Delta\phi_b)|}} \quad . \quad (43)$$

Inserting Eqs.(43) into Eqs.(42), we get the expected scaling of the running couplings with $\ell/\ell_K[\Delta\phi_b]$ [2], that is

$$\begin{aligned} G_{1,2} \left[l = \ln\left(\frac{\ell}{\ell_0}\right) \right] &= G_\Delta |\sin(\Delta\phi_b)| \left\{ \frac{1 + \left(\frac{\ell}{\ell_K[\Delta\phi_b]}\right)^{2G_\Delta |\sin(\Delta\phi_b)|}}{1 - \left(\frac{\ell}{\ell_K[\Delta\phi_b]}\right)^{2G_\Delta |\sin(\Delta\phi_b)|}} \right\} \\ G_{2,3} \left[l = \ln\left(\frac{\ell}{\ell_0}\right) \right] &= G_\Delta |\sin(\Delta\phi_b)| \left\{ \frac{2 \cos(\Delta\phi_b) \left(\frac{\ell}{\ell_K[\Delta\phi_b]}\right)^{G_\Delta |\sin(\Delta\phi_b)|}}{1 - \left(\frac{\ell}{\ell_K[\Delta\phi_b]}\right)^{2G_\Delta |\sin(\Delta\phi_b)|}} \right\} \quad . \end{aligned} \quad (44)$$

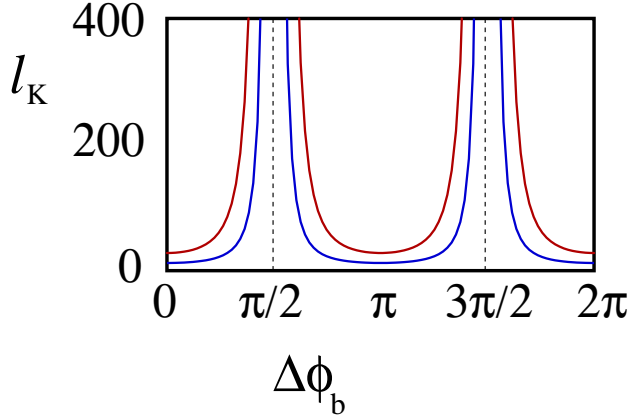


Figure 6: $\ell_K[\Delta\phi_b]$ as a function of $\Delta\phi_b$ for $0 \leq \Delta\phi_b \leq 2\pi$ and for $G_\Delta = 0.3$ (red curve), and for $G_\Delta = 0.4$ (blue curve). Due to the divergence of the right-hand side of Eq.(43) at $\Delta\phi_b = \frac{\pi}{2}, \frac{3\pi}{2}$, the plots have been cutoff around these values of the applied phase difference.

In the specific case discussed here, none of the running couplings changes sign along the RG trajectories. Therefore, rescaling ℓ at fixed $\Delta\phi_b$ does not induce switches in the “actual” groundstate of the system: this either corresponds to the singlet state $|\psi_1\rangle_\gamma$, or to the $M = 0$ component of the triplet, $|\psi_2\rangle_\gamma$, of Eqs.(D.13), depending on whether $\cos(\Delta\phi_b) > 0$, or $\cos(\Delta\phi_b) < 0$. On rescaling ℓ at a given $\Delta\phi_b$, Eqs.(42) imply that $G_{1,2} \left[l = \ln\left(\frac{\ell}{\ell_0}\right) \right]$ and $G_{2,3} \left[l = \ln\left(\frac{\ell}{\ell_0}\right) \right]$ are scaling functions of $\ell/\ell_K[\Delta\phi_b]$, but also that the explicit form of the scaling function parametrically depends on the RG invariant $\kappa[\Delta\phi_b] = [G_{1,2}^{(0)}]^2 - [G_{2,3}^{(0)}]^2 = G_\Delta^2 \sin^2(\Delta\phi_b)$. The key point is that, by simply acting on $\Delta\phi_b$ and/or on G_Δ (that is, on J_Δ), we may change $\ell_K[\Delta\phi_b]$, by leaving the parametric function unchanged (that is, by simultaneously varying the boundary exchange strength J_Δ so that $J_\Delta \sin(\Delta\phi_b)$ does not change). We can vary at will $\ell_K[\Delta\phi_b]$ and therefore recover the pertinent setup to directly probe the (Kondo) scaling by directly tuning $\ell_K[\Delta\phi_b]$. As a probe of the emergence of $\ell_K[\Delta\phi_b]$, we can measure the equilibrium spin current through the junction.

From Eq.(43) we see that $\ell_K[\Delta\phi_b]$ is minimum when $\Delta\phi_b = k\pi$, with integer k . At these values of $\Delta\phi_b$ (and, in general, within small intervals centered on these values), the system rapidly evolves toward the Kondo regime, already for ℓ as large as 30 sites (for $G_\Delta = 0.3$) or even 10 sites (for $G_\Delta = 0.4$). Moving from 0 to larger values of $\Delta\phi_b$, $\ell_K[\Delta\phi_b]$ increases, implying that longer chains are required (larger ℓ), in order for the junction to reach the Kondo regime. Eventually, $\ell_K[\Delta\phi_b]$ diverges at $\Delta\phi_b = \frac{\pi}{2}$ and, by periodicity, at any $\Delta\phi_b = \frac{\pi}{2} + k\pi$, with k integer. This means that, for $\Delta\phi_b$ close to $\frac{\pi}{2} + k\pi$, in practice the junction never reaches the Kondo regime. As a result, we conclude that the same system does, or does not, exhibit Kondo effect depending on just a single parameter, in principle tunable from the outside, such as the value of the angle $\Delta\phi_b$ between the Ising axis in the external leads of chains 1 and 2 and the axis in the external lead of chain 3. To evidence this behavior, in Fig.6 we plot $\ell_K[\Delta\phi_b]$ as a function of $\Delta\phi_b$ for $0 \leq \Delta\phi_b \leq 2\pi$ and for $G_\Delta = 0.3$ (red curve), and for $G_\Delta = 0.4$ (blue curve). Aside from the features above, the plot evidences the $\Delta\phi_b = \pi$ periodicity of $\ell_K[\Delta\phi_b]$, which is implied by Eq.(43), and the over-all decrease of the curves as G_Δ is increased. Due to the divergences at $\Delta\phi_b = \frac{\pi}{2}, \frac{3\pi}{2}$, the plots have been cutoff around these values of the applied phase difference.

To determine the spin currents through the three chains, we differentiate the groundstate energy with respect to the phases $\{\phi_\mu\}$. By substituting, in Eq.(27), the bare boundary coupling strengths with the renormalized ones, we obtain, at generic values of $\Delta\phi_a, \Delta\phi_b$, the ℓ -dependent energy

$$\mathcal{E}^{(0)}[\ell; \Delta\phi_a, \Delta\phi_b] = -\frac{v}{\ell+1} \max_{\lambda_a, \lambda_b = \pm 1} \{ \lambda_a G_{1,2}[\ell; \Delta\phi_a, \Delta\phi_b] + \lambda_b G_{2,3}[\ell; \Delta\phi_a, \Delta\phi_b] + \lambda_a \lambda_b G_{3,1}[\ell; \Delta\phi_a, \Delta\phi_b] \}, \quad (45)$$

with the dependence of the running couplings on the scale ℓ and on $\Delta\phi_a, \Delta\phi_b$ explicitly evidenced. Taking into account that $\Delta\phi_a, \Delta\phi_b$ enter the explicit formulas for the running couplings only through the $G_{\lambda, \lambda+1}^{(0)}$'s, we readily recover the formulas for the currents through the three chains, which are given by

$$I_\mu[\ell; \Delta\phi_a, \Delta\phi_b] = \frac{vG_\Delta \sin[\phi_\mu - \phi_{\mu+1}]}{\ell+1} \sum_{\lambda=1}^3 \frac{\partial \hat{G}_{\lambda, \lambda+1}}{\partial G_{\mu, \mu+1}^{(0)}} - \frac{vG_\Delta \sin[\phi_{\mu-1} - \phi_\mu]}{\ell+1} \sum_{\lambda=1}^3 \frac{\partial \hat{G}_{\lambda, \lambda+1}}{\partial G_{\mu-1, \mu}^{(0)}}, \quad (46)$$

with $\hat{G}_{3,1} = \lambda_a \lambda_b G_{3,1}$, $\hat{G}_{1,2} = \lambda_a G_{1,2}$, $\hat{G}_{2,3} = \lambda_b G_{2,3}$. In our specific case, taking into account the system symmetries, we obtain

$$I_1[\ell; \Delta\phi_b] = I_2[\ell; \Delta\phi_b] = \frac{vG_\Delta \sin(\Delta\phi_b)}{\ell+1} \sum_{\lambda=1}^3 \frac{\partial \hat{G}_{\lambda, \lambda+1}}{\partial G_{3,1}^{(0)}} \\ I_3[\ell; \Delta\phi_b] = -2I_1[\ell; \Delta\phi_b] = -\frac{vG_\Delta \sin(\Delta\phi_b)}{\ell+1} \sum_{\lambda=1}^3 \left\{ \frac{\partial \hat{G}_{\lambda, \lambda+1}}{\partial G_{3,1}^{(0)}} + \frac{\partial \hat{G}_{\lambda, \lambda+1}}{\partial G_{2,3}^{(0)}} \right\} = \frac{v}{\ell+1} \sum_{\lambda=1}^3 \frac{\partial \hat{G}_{\lambda, \lambda+1}}{\partial \Delta\phi_b} \quad (47)$$

Clearly, the onset of the nonperturbative regime in the running couplings implies, via Eqs.(47), an analogous feature in the equilibrium spin currents. This can be detected by two alternative means, that is, by either looking at the scaling of $I_\mu[\ell; \Delta\phi_b]$ as a function of ℓ at a given $\Delta\phi_b$, or by looking at the current pattern throughout the whole interval of periodicity in $\Delta\phi_b$ at different (and increasing) values of $\Delta\phi_b$.

Within the former approach, we expect to see the onset of the nonperturbative regime in the spin current that takes place at different scales ℓ for different values of $\Delta\phi_b$, reflecting the dependence of ℓ_K on $\Delta\phi_b$. To verify such a prediction, in Fig.7 we present logarithmic plots of $I_1[\ell; \Delta\phi_b]/I_1[\ell_0; \Delta\phi_b]$ as a function of ℓ at fixed $\Delta\phi_b (= 0.1\pi, 0.2\pi, 0.3\pi, 0.4\pi)$, and for two different values of G_Δ , as detailed in the figure caption. The smallest value of $\Delta\phi_b$ we use to draw Fig.7a) and Fig.7b) is $\Delta\phi_b = 0.1\pi$. To obtain readable plots, we therefore draw diagrams up to a maximum value of ℓ slightly lower than $\ell_K[\Delta\phi_b = 0.1\pi]$, which is $\sim 170\ell_0$ for $G_\Delta = 0.2$ (Fig.7a)) and $\sim 27\ell_0$ for $G_\Delta = 0.3$ (Fig.7b)). As expected, we see that, on increasing $\Delta\phi_b$ from values close to 0 to values close to $\frac{\pi}{2}$, the current plots evolve from diagrams exhibiting a clear upturn for $\Delta\phi_b = 0.1\pi$ at a scale $\ell \sim \ell_K[0.1\pi]$, to a simple decrease with ℓ roughly $\propto \ell^{-1}$ times corrections from higher-order contributions in the boundary couplings at $\Delta\phi_b = 0.4\pi$. Given our result for $\ell_K[\Delta\phi_b]$, we may therefore readily interpret Fig.7a) and Fig.7b) as an evidence for $\ell_K[\Delta\phi_b]$ to increase at $\Delta\phi_b$ increasing from 0 to $\frac{\pi}{2}$. This is, in fact, a striking feature of our system: by just acting on $\Delta\phi_b$ keeping all the other system parameters fixed, we may tune, or not, the onset of the Kondo regime at a given scale, given the large window of variation of $\ell_K[\Delta\phi_b]$ evidenced in Fig.6.

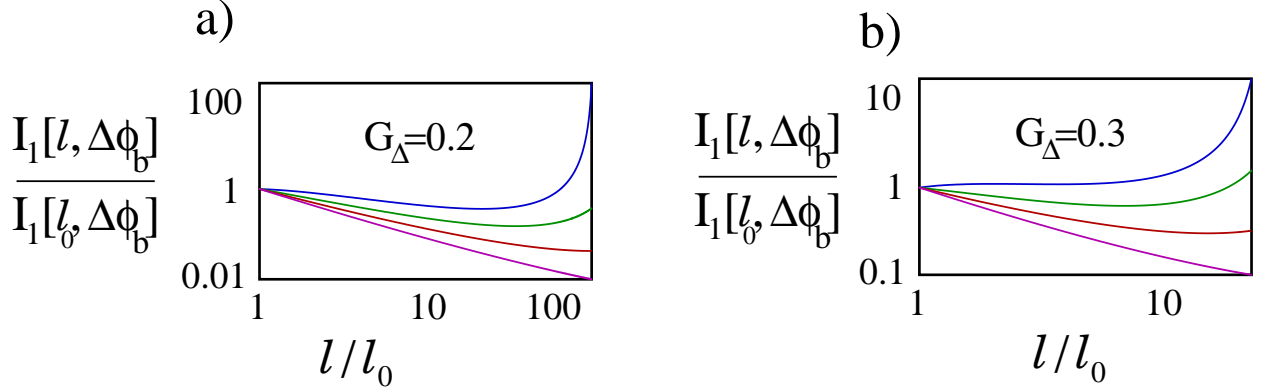


Figure 7: **a)** $I_1[l; \Delta\phi_b]/I_1[l_0; \Delta\phi_b]$ as a function of l/l_0 for $G_\Delta = 0.2$ and for (from top to bottom) $\Delta\phi_b = 0.1\pi$ (blue curve), $\Delta\phi_b = 0.2\pi$ (green curve), $\Delta\phi_b = 0.3\pi$ (red curve), $\Delta\phi_b = 0.4\pi$ (magenta curve). The increase of $\ell_K[\Delta\phi_b]$ with $\Delta\phi_b$ as the phase difference evolves from 0 to $\frac{\pi}{2}$ is apparent in the switch of the upturn of the curve as $l \sim 100\ell_0$ for $\Delta\phi_b = 0.1\pi$ to a (roughly) ℓ^{-1} scaling at $\Delta\phi_b = 0.4\pi$, which is what we would expect in the absence of a Kondo-like boundary interaction; **b)** Same as in panel **a)**, but with $G_\Delta = 0.3$.

To complement the results reported in Fig.7, we may alternatively analyze $I_1[l; \Delta\phi_b]$ as a function of $\Delta\phi_b$ at fixed chain length, for different values of l . Since the scaling of $I_1[l; \Delta\phi_b]$ with l is different for different values of $\Delta\phi_b$, as we discuss above, we expect that monitoring the spin current across a full periodicity interval at increasing values of l , the growth of the current with l is faster in the regions of values of $\Delta\phi_b$ where $\ell_K[\Delta\phi_b]$ is lower. An important point here is that, differently from the previous analysis, now the plots are drawn by varying $\Delta\phi_b$ at fixed l . Thus, the question arises whether, at a groundstate level crossing of the junction triggered by the change in $\Delta\phi_b$, the system “adiabatically” keeps within the same state, or whether, at the level crossing, it “jumps” back into its actual groundstate. Apparently, this issue bears a close resemblance with the fermion parity conservation which we discuss in Sec.3 in the context of the $N = 2$ junction. However, as we evidence in Appendix D, it is possible to realize singlet, as well as triplet, groundstates at either value of the total fermion parity. In our specific case, starting from $\Delta\phi_b = 0$ and increasing the phase difference, from Eqs.(42), we see that all three the $G_{\mu,\mu+1}$ ’s keep > 0 as long as $0 \leq \Delta\phi_b < \frac{\pi}{2}$. Therefore, in this range of values of $\Delta\phi_b$, the junction groundstate corresponds to the singlet $|\psi_1\rangle_\gamma$ of Eq.(D.13), with $\gamma = \pm 1$. Accordingly, the spin currents are given by Eqs.(47) with $\hat{G}_{\mu,\mu+1} = G_{\mu,\mu+1}$. At $\Delta\phi_b = \frac{\pi}{2}$ a level crossing takes place in the junction groundstate between $|\psi_1\rangle_\gamma$ and the $|\psi_2\rangle_\gamma$ component of the triplet. Correspondingly, the spin currents are still given by Eqs.(47), with $\hat{G}_{2,3} = -G_{2,3}$ and $\hat{G}_{3,1} = -G_{3,1}$. Whether, when going across the level crossing, the system keeps within $|\psi_1\rangle_\gamma$, or it switches to $|\psi_2\rangle_\gamma$, may depend on a number of factors, such as, for instance, how “adiabatically” we vary $\Delta\phi_b$. For what concerns the spin current pattern, just as it happens for the $N = 2$ junction, a switch in the groundstate at $\Delta\phi_b = \frac{\pi}{2}$ determines a finite discontinuity in the currents and a corresponding halving of the period in $\Delta\phi_b$. To evidence the main features of the spin current in both cases, in Fig.8 we plot the current I_1 as a function of $\Delta\phi_b$ for $G_\Delta = 0.2$ by both assuming that the system is always able to relax into the actual groundstate (Fig.8a) - note that the period in this case is halved and $= \pi$ -) and by assuming that the system does not relax and keeps within the same state when we go across $\Delta\phi_b = \frac{\pi}{2}, \frac{3\pi}{2}$

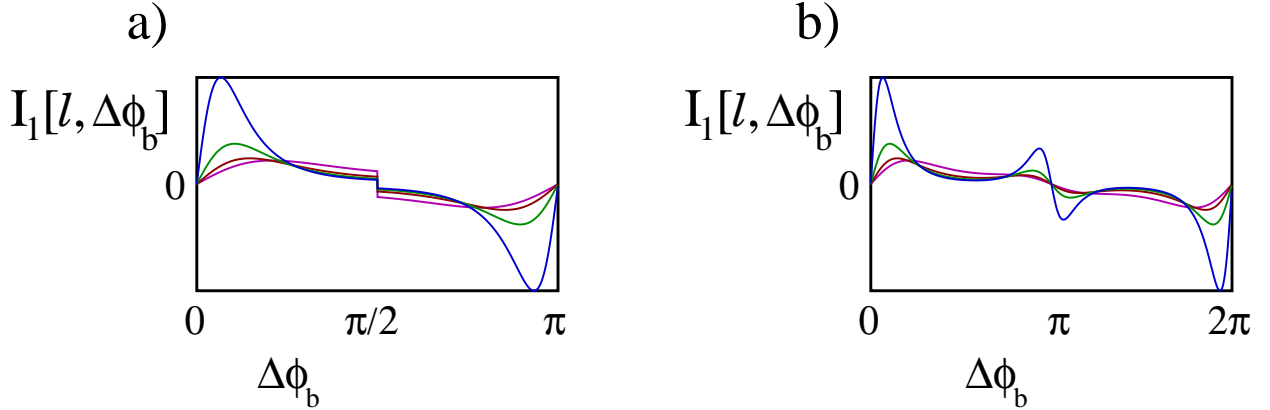


Figure 8: **a)** $I_1[l; \Delta\phi_b]$ as a function of $\Delta\phi_b$ for $G_\Delta = 0.2$ and for (from top to bottom) $\frac{\ell}{\ell_0} = 120$ (blue curve), $\frac{\ell}{\ell_0} = 90$ (green curve), $\frac{\ell}{\ell_0} = 60$ (red curve), $\frac{\ell}{\ell_0} = 30$ (magenta curve). The plots have been drawn by assuming that the system always occupies its true groundstate, which determines the finite jump in the current at $\Delta\phi_b = \frac{\pi}{2}$ and the halving of the period to π ; **b)** Same as in panel **a)**, but in this case it is assumed that the system does not relax to its actual groundstate when $\Delta\phi_b$ crosses $\frac{\pi}{2}$ and $\frac{3\pi}{2}$.

(Fig.8**b)**). Aside from the differences in the discontinuity at $\frac{\pi}{2}$ and in the over-all period, the two plots share the same feature. Specifically, in both cases we see that, on increasing ℓ , the current is enhanced around the values of $\Delta\phi_b$ at which $\ell_K[\Delta\phi_b]$ is minimum, that is, $\Delta\phi_b = 0, \pi, 2\pi$, due to the onset of the Kondo regime. At variance, around $\Delta\phi_b = \frac{\pi}{2}, \frac{3\pi}{2}$, where $\ell_K[\Delta\phi_b]$ is maximum, the lead length is consistently smaller than the corresponding value of ℓ_K , the Kondo effect does not set in and, as a result, the current decreases with ℓ roughly as ℓ^{-1} , as it would be appropriate in the absence of Kondo effect.

For the sake of completeness, we now briefly discuss a different situation, still easily tractable analytically, corresponding to $\phi_1 = -\phi_2 = \frac{\Delta\phi_a}{2}$, $\phi_3 = 0$. In this case, we obtain

$$G_{1,2}^{(0)} = G_\Delta \cos(\Delta\phi_a) \quad , \quad G_{2,3}^{(0)} = G_{3,1}^{(0)} = G_\Delta \cos\left(\frac{\Delta\phi_a}{2}\right) \quad . \quad (48)$$

Pointing out that now, on letting the phase $\phi_1(\phi_2)$ go through a full period, we get that the result must be periodic in $\Delta\phi_a$ with period equal to 4π , we note that, regardless of the specific sign of the boundary couplings, to analytically solve the problem it is useful to separately treat the case $|\cos(\Delta\phi_a)| < \left|\cos\left(\frac{\Delta\phi_a}{2}\right)\right|$, which corresponds to $0 < \Delta\phi_a < \frac{2\pi}{3}$, to $\frac{4\pi}{3} < \Delta\phi_a < 8\pi/3$, and to $10\pi/3 < \Delta\phi_a < 4\pi$, and the case $|\cos(\Delta\phi_a)| > \left|\cos\left(\frac{\Delta\phi_a}{2}\right)\right|$, which corresponds to $\frac{2\pi}{3} < \Delta\phi_a < \frac{4\pi}{3}$ and $8\pi/3 < \Delta\phi_a < 10\pi/3$. In the former case, the running couplings are given by

$$G_{1,2} \left[l = \ln\left(\frac{\ell}{\ell_0}\right) \right] = G_\Delta \Omega(\Delta\phi_a) \tan \left\{ \arctan \left[\frac{\cos(\Delta\phi_a)}{\Omega(\Delta\phi_a)} \right] + G_\Delta \Omega(\Delta\phi_a) \ln\left(\frac{\ell}{\ell_0}\right) \right\}$$

$$G_{2,3} \left[l = \ln\left(\frac{\ell}{\ell_0}\right) \right] = \frac{G_\Delta \Omega(\Delta\phi_a) \epsilon \left[\cos\left(\frac{\Delta\phi_a}{2}\right) \right]}{\cos \left\{ \arctan \left[\frac{\cos(\Delta\phi_a)}{\Omega(\Delta\phi_a)} \right] + G_\Delta \Omega(\Delta\phi_a) \ln\left(\frac{\ell}{\ell_0}\right) \right\}} \quad , \quad (49)$$

with $\Omega(\Delta\phi_a) = \sqrt{\cos^2\left(\frac{\Delta\phi_a}{2}\right) - \cos^2(\Delta\phi_a)}$ and $\epsilon(\phi)$ being the sign function, and, clearly, $G_{2,3}\left[l = \ln\left(\frac{\ell}{\ell_0}\right)\right] = G_{3,1}\left[l = \ln\left(\frac{\ell}{\ell_0}\right)\right]$.

Eqs.(49) imply that the running couplings diverge (either by positive, or negative values), at a scale $\ell_K[\Delta\phi_a]$ given by [39, 35]

$$\ell_K[\Delta\phi_a] = \ell_0 \exp\left\{\left[\frac{1}{G_\Delta\Omega(\Delta\phi_a)}\right]\left[\frac{\pi}{2} - \arctan\left[\frac{\cos(\Delta\phi_a)}{\Omega(\Delta\phi_a)}\right]\right]\right\}. \quad (50)$$

As stated in Appendix Appendix E, we expect that, for $0 \leq \Delta\phi_a \leq \frac{2\pi}{3}$, the junction flows towards the Kondo fixed point with all the three running coupling flowing to $+\infty$ (after a change in sign of $G_{1,2}$ along the renormalization group trajectories, if $G_{1,2}^{(0)} < 0$), and that the same thing happens for $\frac{10\pi}{3} \leq \Delta\phi_a \leq 2\pi$. Eq.(50) implies that $\ell_K[\Delta\phi_a] \rightarrow \infty$ for $\Delta\phi_a \rightarrow \frac{2\pi}{3}^-$, as well as for $\Delta\phi_a \rightarrow \frac{10\pi}{3}^-$. Therefore, we conclude that no crossover to Kondo regime can in practice take place close to those boundaries of the intervals of validity of Eqs.(49).

In the complementary case, $\frac{2\pi}{3} < \Delta\phi_a < \frac{4\pi}{3}$ and $8\pi/3 < \Delta\phi_a < 10\pi/3$, we obtain

$$\begin{aligned} G_{1,2}\left[l = \ln\left(\frac{\ell}{\ell_0}\right)\right] &= G_\Delta \tilde{\Omega}(\Delta\phi_a) \left\{ \frac{\cos(\Delta\phi_a) + \tilde{\Omega}(\Delta\phi_a) + [\cos(\Delta\phi_a) - \tilde{\Omega}(\Delta\phi_a)]\left(\frac{\ell}{\ell_0}\right)^{2G_\Delta\tilde{\Omega}(\Delta\phi_a)}}{\cos(\Delta\phi_a) + \tilde{\Omega}(\Delta\phi_a) - [\cos(\Delta\phi_a) - \tilde{\Omega}(\Delta\phi_a)]\left(\frac{\ell}{\ell_0}\right)^{2G_\Delta\tilde{\Omega}(\Delta\phi_a)}} \right\} \\ G_{2,3}\left[l = \ln\left(\frac{\ell}{\ell_0}\right)\right] &= G_\Delta \tilde{\Omega}(\Delta\phi_a) \left\{ \frac{2 \cos\left(\frac{\Delta\phi_a}{2}\right)\left(\frac{\ell}{\ell_0}\right)^{G_\Delta\tilde{\Omega}(\Delta\phi_a)}}{\cos(\Delta\phi_a) + \tilde{\Omega}(\Delta\phi_a) - [\cos(\Delta\phi_a) - \tilde{\Omega}(\Delta\phi_a)]\left(\frac{\ell}{\ell_0}\right)^{2G_\Delta\tilde{\Omega}(\Delta\phi_a)}} \right\} \end{aligned} \quad (51)$$

with $\tilde{\Omega}(\Delta\phi_a) = \sqrt{\cos^2(\Delta\phi_a) - \cos^2\left(\frac{\Delta\phi_a}{2}\right)}$.

From the right-hand side of Eqs.(51), we readily see that, whenever $\cos(\Delta\phi_a) < 0$, there is no onset of the Kondo regime at the junction. Indeed, since $\cos\left(\frac{\Delta\phi_a}{2}\right) < 0$ for $\frac{2\pi}{3} < \Delta\phi_a < \frac{10\pi}{3}$, having $\cos(\Delta\phi_a) < 0$ corresponds to the case $G_{2,3}^{(0)} = G_{3,1}^{(0)}$ and $G_{\lambda,\lambda+1}^{(0)} < 0, \forall \lambda$. As we discuss in detail in Appendix Appendix E, no Kondo effect is expected to set in this case, which is ultimately consistent with Eqs.(51). At variance, the crossover to the Kondo regime takes place when $\cos(\Delta\phi_a) > 0$, with an associated Kondo length $\ell_K[\Delta\phi_a]$ given by

$$\ell_K[\Delta\phi_a] = \left\{ \frac{\cos(\Delta\phi_a) + \tilde{\Omega}(\Delta\phi_a)}{\cos(\Delta\phi_a) - \tilde{\Omega}(\Delta\phi_a)} \right\}^{\frac{1}{2G_\Delta\tilde{\Omega}(\Delta\phi_a)}}. \quad (52)$$

We therefore conclude that both Eqs.(42) and Eqs.(49,51) are consistent with the general RG analysis of Appendix Appendix E, of which they constitute a special case. In both cases, analyzing the scaling properties of the equilibrium spin currents through the junction provides an effective tool to map out the phase diagram associated to the corresponding RG trajectories. For the sake of simplicity, here we do not discuss further our second example, as the corresponding analysis would be exactly analogous to what we have done in the first example.

As a general comment on the emerging TKE at our YSC, it is worth stressing that, differently from what happens with Y junctions of fermionic quantum wires [62, 63] and of Josephson

junction chains [64, 42, 53], here we recover a nontrivial phase diagram for the junction even in the absence of a bulk interaction in the chain. This is a remarkable effect of the Kondo interaction, which is marginally relevant and is able to take the system out of the trivial, weakly coupled regime, even with effectively (in terms of JW fermions) noninteracting leads.

7. Conclusions

In this paper we have derived the topological Kondo Hamiltonian describing a Y junction of three inhomogeneous spin chains in which the inner XX-spin chains are connected to each other at their inner boundary, while, at the outer boundary, they are connected to quantum Ising chains with different tilting angles for the Ising axis. Mapping the system Hamiltonian onto a pertinent boundary model, we have shown that the tilting angles effectively act as phases applied to the XX chains, thus triggering a nontrivial equilibrium spin current pattern through the junction.

Employing the renormalization group approach to this topological Kondo model, we have been able to express the running couplings as functions of the bare couplings and of the running scale. Substituting the corresponding formulas in the expression of the system groundstate energy, we have eventually derived the energy itself at a generic value of the running scale l as a function of l and of the applied phases. This allowed us to derive scaling formulas for the spin currents, by simply differentiating the running groundstate energy with respect to the applied phases. We have therefore argued how it is possible to directly measure the Kondo screening length ℓ_K by monitoring the crossover in the currents induced by the onset of the Kondo regime.

Along our derivation, as evidenced by the examples we provide in Sec.6, we have shown that ℓ_K is a known function of the applied phases. This has provided us with two complementary ways to probe the Kondo length, by either looking at the scaling of the currents with l at fixed applied phases, or by fixing l and tuning ℓ_K by varying the applied phases.

Incidentally, it is worth stressing how our proposed YSC is likely to be within the reach of nowadays technology, both for what concerns the practical realization of the system we propose, as well as regarding the experimental probe of the spin currents. In principle, it could be realized by means of, e.g., Josephson junction arrays, which are well-known to effectively behave as quantum spin chains with the properties required to realize our YSC [52, 33, 65]. Also, several effective methods to efficiently detect the spin currents through the junction are already potentially available to experimentalists as extensively discussed in, e.g., Ref.[43].

To summarize our results, we have shown how a $N = 3$ YSC provides a rather unique Kondo setting in which we may easily tune the Kondo length by acting on the phase differences only. Tuning the Kondo length allows for mapping out the scaling properties of the system without, e.g., changing the length of the chains and/or varying the energy/temperature scale(s) associated to the measurement, which should not be easy to do in a realistic system, thus paving the way to the possibility of a clear-cut experimental measurement of the so far pretty elusive Kondo scaling length [23].

Acknowledgements – A. N. was financially supported by POR Calabria FESR-FSE 2014/2020 - Linea B) Azione 10.5.12, grant no. A.5.1. D. G. acknowledges financial support from Italy’s MIUR PRIN project TOP-SPIN (Grant No. PRIN 20177SL7HC).

Appendix A. Derivation of the effective boundary Hamiltonian for the topological superconductor-normal wire junction

In this Appendix we recover, in terms of JW fermions, the effective boundary Hamiltonian corresponding to H_{SC}^λ in Eq.(1).

In particular, the boundary Hamiltonian exactly describes the interface between the XX-chain and the outer Ising chain in the limit $\gamma = t$ and $g = 0$ [50]. As a result, we obtain

$$\begin{aligned} & -t \sum_{j=\ell+1}^{L-1} \{c_{j,\lambda}^\dagger c_{j+1,\lambda} + c_{j+1,\lambda}^\dagger c_{j,\lambda}\} - \gamma \sum_{j=\ell+1}^{L-1} \{c_{j,\lambda} c_{j+1,\lambda} e^{-2i\phi_\lambda} + c_{j+1,\lambda}^\dagger c_{j,\lambda}^\dagger e^{2i\phi_\lambda}\} - g \sum_{j=\ell+1}^L c_{j,\lambda}^\dagger c_{j,\lambda} \\ & \rightarrow -t \sum_{j=\ell+1}^{L-1} \{[c_{j,\lambda}^\dagger e^{i\phi_\lambda} + c_{j,\lambda} e^{-i\phi_\lambda}][c_{j+1,\lambda} e^{-i\phi_\lambda} - c_{j+1,\lambda}^\dagger e^{i\phi_\lambda}]\} \equiv -it \sum_{j=\ell+1}^{L-1} \xi_{j,\lambda} \eta_{j+1,\lambda} \quad , \end{aligned} \quad (\text{A.1})$$

with the real lattice fermions $\xi_{j,\lambda}, \eta_{j,\lambda}$ respectively given by

$$\begin{aligned} \xi_{j,\lambda} &= c_{j,\lambda} e^{-i\phi_\lambda} + c_{j,\lambda}^\dagger e^{i\phi_\lambda} \\ \eta_{j,\lambda} &= -i \{c_{j,\lambda} e^{-i\phi_\lambda} - c_{j,\lambda}^\dagger e^{i\phi_\lambda}\} \quad . \end{aligned} \quad (\text{A.2})$$

Defining new, ‘‘nonlocal’’ Dirac fermions $d_{j,\lambda}$ ($j = \ell + 1, \dots, L - 1$) as $d_{j,\lambda} = \frac{1}{2} \{\xi_{j,\lambda} - i\eta_{j+1,\lambda}\}$, we find that

$$-it \sum_{j=\ell+1}^{L-1} \xi_{j,\lambda} \eta_{j+1,\lambda} = 2t \sum_{j=\ell+1}^{L-1} \left[d_{j,\lambda}^\dagger d_{j,\lambda} - \frac{1}{2} \right] \quad , \quad (\text{A.3})$$

which evidences the emergence of the zero-mode operators at the two endpoints, respectively given by

$$\begin{aligned} \eta_{\ell+1,\lambda} &= -i \{c_{\ell+1,\lambda} e^{-i\phi_\lambda} - c_{\ell+1,\lambda}^\dagger e^{i\phi_\lambda}\} \\ \xi_{L,\lambda} &= c_{L,\lambda}^\dagger e^{i\phi_\lambda} + c_{L,\lambda} e^{-i\phi_\lambda} \quad . \end{aligned} \quad (\text{A.4})$$

Finally, we project the term in the model Hamiltonian that is \propto to J' in Eq.(2) onto the subspace spanned by the zero-modes in Eq.(A.4), thus obtaining the boundary Hamiltonian $H_{B,\lambda}$, given by

$$H_{B,\lambda} = i\frac{\tau}{2} \gamma_\lambda \{e^{-i\phi_\lambda} c_{\ell,\lambda} + e^{i\phi_\lambda} c_{\ell,\lambda}^\dagger\} \quad , \quad (\text{A.5})$$

with $\gamma_\lambda \equiv \eta_{\ell+1,\lambda}$ and $\tau \propto J'$. Based on the derivation illustrated in this Appendix, throughout all the paper we used as effective fermionic realization of the model Hamiltonian for each spin-chain the Hamiltonian $H_{F,\lambda}$, given by

$$H_{F,\lambda} = -J \sum_{j=1}^{\ell-1} \{c_{j,\lambda}^\dagger c_{j+1,\lambda} + c_{j+1,\lambda}^\dagger c_{j,\lambda}\} - H \sum_{j=1}^{\ell} c_{j,\lambda}^\dagger c_{j,\lambda} + H_{B,\lambda} \quad , \quad (\text{A.6})$$

with $H_{B,\lambda}$ given in Eq.(A.5).

At generic values of the system parameters, the boundary model provides a reliable approximation at energies $\leq \Delta_{\text{Eff}}$, with the effective gap $\Delta_{\text{Eff}} \sim |2t - g|$, in which case we effectively describe the interface by retaining the low-energy emerging Majorana mode as the only effective degree of freedom on the gapped side [44, 45].

Appendix B. Periodicity in the spin equilibrium current through a single chain with an even/odd number of sites ℓ

In Sec.2 we mentioned how, for a single inhomogeneous chain, corresponding to an $N = 2$ junction, the periodicity of the spin equilibrium current is expected to depend on whether the number of sites in the chain, ℓ , is even, or odd [43]. Since, throughout all the paper, we focus onto symmetric junctions only, which behave as the even- ℓ chain, in the following we consider also chains with odd ℓ .

For the sake of completeness and also to allow for a detailed comparison of our results with the ones obtained in Ref.[43], we devote this Appendix to carefully investigate how the periodicity in a single chain depends on whether ℓ is even, or odd. In doing so, we relate the current periodicity to the structure of the low-lying energy eigenmodes of the chain Hamiltonian and to their dependence on the applied phase difference.

To simplify our discussion, here we consider the simple model for the $N = 2$ junction, that is, a single, homogeneous chain, connected to two Ising chains at its endpoints, with tilting angles corresponding to phases ϕ_1 and ϕ_2 .

According to the derivation of Appendix A, we describe the chain in terms of the lattice boundary Hamiltonian $H_2 = H_{\text{Bulk}}^{(2)} + H_B$, with

$$H_{\text{Bulk}}^{(2)} = -J \sum_{j=1}^{\ell-1} \{c_j^\dagger c_{j+1} + c_{j+1}^\dagger c_j\} - \mu \sum_{j=1}^{\ell} c_j^\dagger c_j$$

$$H_B = i\frac{\tau}{2}\gamma_1 \{e^{-i\phi_1} c_1 + e^{i\phi_1} c_1^\dagger\} + i\frac{\tau}{2}\gamma_2 \{e^{-i\phi_2} c_\ell + e^{i\phi_2} c_\ell^\dagger\} . \quad (\text{B.1})$$

By exactly diagonalizing H_2 at fixed phase difference $\phi_1 - \phi_2$, we have computed the spin current $I[\phi] = I[\phi_1 - \phi_2]$ when $\mu = 0$ and $\tau/J = 0.25$, for $\ell = 40$ and for $\ell = 41$.

We draw the relevant plots in Fig.B.9, which we have constructed assuming that fermion parity is always preserved. For $\ell = 40$ (Fig.B.9a), the system realizes the so-called \mathcal{Z}_2 -periodicity, with the current periodic, with period equal to 2π . Correspondingly, there are two branches for the spin supercurrent $I[\phi]$. For $\ell = 41$ (Fig.B.9b), the system realizes the \mathcal{Z}_4 -periodicity, with the current periodic with period equal to 4π , and four different branches.

To provide a physical interpretation of the current plots in Fig.B.9, in Fig.B.10 we show the single-quasiparticle energy levels crossing the Fermi level as ϕ varies. Fig.B.10a) and Fig.B.10b) are drawn for systems with the same parameters as the ones corresponding to Fig.B.9a) and to Fig.B.9b).

Let us focus on Fig.B.10a) first. With the green and the red dots we mark the levels that are nearest neighbors to the ones that cross as ϕ varies. In this case, they play no role in determining the behavior of $I[\phi]$. At variance, what matters is the position of the levels that we mark with respectively a blue and a black dot with respect to the Fermi level, which we mark with a dashed green line. We see that, as long as $\phi < \frac{\pi}{2}$, the groundstate is determined by a pair of a black and a green dot. This corresponds to a given fermion parity, say $+1$. As ϕ crosses $\frac{\pi}{2}$, the new groundstate is determined by a pair of a blue and a green dot, which corresponds to the filled (with one additional fermion) level close to the Fermi energy becoming lower in energy than the

corresponding empty one (the black dot), with a net change in the fermion parity of the system, that now has become -1 . The fermion parity keeps -1 till $\phi = \frac{3\pi}{2}$, which corresponds to the region we mark with 2 in Fig.B.10a). Then, it becomes again $+1$. Clearly, requiring fermion parity to be conserved means that the system groundstate, at any value of ϕ , always corresponds to either a black and a green dot, or to a blue and a green dot, which implies two branches in the total current and a total periodicity of 2π . As highlighted by our discussion, this behavior is strictly related to the dynamics of the two low-lying states, related to each other by a \mathcal{Z}_2 -transformation, and is accordingly dubbed \mathcal{Z}_2 -periodicity of the current.

Let us now consider Fig.B.10b). In this case, which corresponds to $\ell = 41$, we have four single-quasiparticle energy level that cross, at various values of ϕ , the Fermi level. In different intervals of values of ϕ (this time ranging from $\phi = 0$ to $\phi = 4\pi$), there are four possible branches, corresponding to the different pairs of colored dot that characterize the system state, which imply the four different branches for $I(\phi)$ in Fig.B.9b). Differently from the even- ℓ case, now the system behavior is related to the dynamics of the four low-lying states, which are mapped onto each other by means of pertinent \mathcal{Z}_4 -transformations, and the (4π) periodicity of $I(\phi)$ is accordingly dubbed \mathcal{Z}_4 -periodicity of the current.

To understand the behavior of the system for ℓ odd, we consider as a reference limit the one in which the boundary Majorana modes are fully decoupled from the rest of the chain (that is, the $\tau \rightarrow 0$ -limit). Here, when ℓ is odd and the chemical potential $\mu = 0$, we find two different Dirac zero-mode operators, the former being determined by a linear combination of γ_1 and γ_2 as $a = \frac{1}{2}(\gamma_1 + i\gamma_2)$, the latter being given by b , with

$$b = \sqrt{\frac{2}{\ell + 1}} \sum_{j=1}^{\ell} (-1)^j c_j \quad . \quad (\text{B.2})$$

On turning on τ and on varying ϕ , a and b , together with their Hermitean conjugate, a and b combine together to determine the fermion low-lying states that cross with each other in Fig.B.9b), which explain why, for ℓ odd, one obtains four different branches for the spin current, rather than two [43]. Incidentally, before concluding this Appendix, it is worth pointing out the striking similarity between our Figs.B.9,B.10 and the plots derived in Ref.[43] under similar conditions, but using the “full” model Hamiltonian (including the leads). Apparently, this is another piece of evidence of the reliability of our simplified boundary model to correctly recover the spin supercurrent in the large- ℓ limit. Incidentally, we also note that, given the system parameters we are considering, the boundary model already describes well the spin current dynamics at ℓ as large as 10, which evidences the high level of reliability of our boundary model Hamiltonian to describe the current pattern through the junction.

Appendix C. Low-energy, long-wavelength effective field theory for the Jordan-Wigner fermion operators

In this Appendix we describe the low-energy, long-wavelength field theory description of the JW fermion operators which we used throughout our paper to discuss the boundary interaction at the junction between the XX-chains and the outer Ising spin chains. To do so, we start by

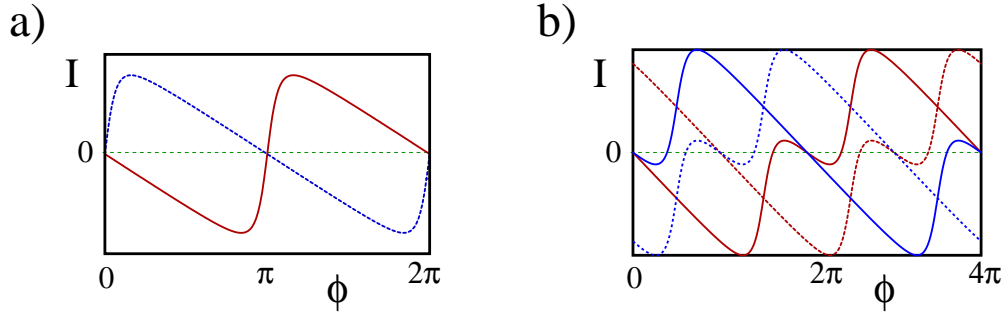


Figure B.9: **a)** Current $I[\phi]$ vs. ϕ in the boundary model with Hamiltonian H_2 for $\tau/J = 0.25$ and $\ell = 40$; **b)** Same as in **a)**, but drawn for $\ell = 41$.

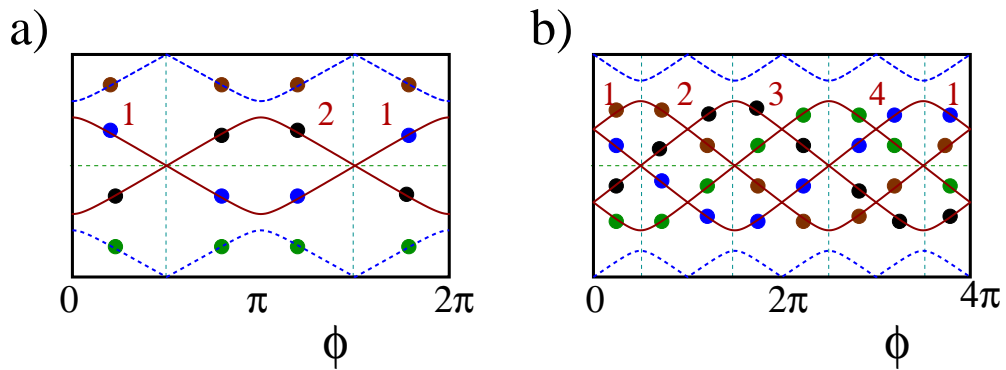


Figure B.10: **a)** Plot of the single-particle levels (solid red lines) closest to the Fermi level (dashed green line) as a function of ϕ in the boundary model with Hamiltonian H_2 for $\tau/J = 0.25$ and $\ell = 40$ as a function of ϕ . Varying ϕ from 0 to 2π , there are two crossings between many-body groundstates with different total fermion parity, marked by the vertical, dashed cyan lines. The regions with different fermion parities are labelled by 1 and 2 in the plot; **b)** Same as in **a)**, but drawn for $\ell = 41$. As ϕ varies from 0 to 4π there are now four different regions (see discussion in the main text), corresponding to a doubled (\mathbb{Z}_4) periodicity in $I[\phi]$ and to the emergence of four different branches in the current.

decomposing the lattice fermion operators in the basis of the eigenmodes of $H = H_{\text{Bulk}} + H_{\Delta}$, $\Gamma_{\epsilon;A}$. Using the additional label A to discriminate between independent eigenmodes corresponding to the same energy ϵ , we set

$$\Gamma_{\epsilon;A} = \sum_{\lambda=1}^N \sum_{j=1}^{\ell} \{u_{j,\epsilon,(A;\lambda)}^* c_{j,\lambda} + v_{j,\epsilon,(A;\lambda)}^* c_{j,\lambda}^{\dagger}\} + \sum_{\lambda=1}^N w_{\epsilon,(A;\lambda)} \gamma_{\lambda} \quad , \quad (\text{C.1})$$

with $\{u_{j,\epsilon,(A;\lambda)}, v_{j,\epsilon,(A;\lambda)}, w_{\epsilon,(A;\lambda)}\}$ being the BDG eigenfunctions for the state A with energy ϵ .

On imposing the canonical commutation relation $[\Gamma_{\epsilon;A}, H] = \epsilon \Gamma_{\epsilon;A}$, we find the BDG that, for $1 < j < \ell$, are given by

$$\begin{aligned} \epsilon u_{j,\epsilon,(A;\lambda)} &= -J \{u_{j+1,\epsilon,(A;\lambda)} + u_{j-1,\epsilon,(A;\lambda)}\} - H u_{j,\epsilon,(A;\lambda)} \\ \epsilon v_{j,\epsilon,(A;\lambda)} &= J \{v_{j+1,\epsilon,(A;\lambda)} + v_{j-1,\epsilon,(A;\lambda)}\} + H v_{j,\epsilon,(A;\lambda)} \quad . \end{aligned} \quad (\text{C.2})$$

For $j = \ell$, we get

$$\begin{aligned} \epsilon u_{\ell,\epsilon,(A;\lambda)} &= -J u_{\ell-1,\epsilon,(A;\lambda)} - H u_{\ell,\epsilon,(A;\lambda)} + \frac{i\tau}{2} e^{-i\phi_{\lambda}} w_{\epsilon,(A;\lambda)} \\ \epsilon v_{\ell,\epsilon,(A;\lambda)} &= J v_{\ell-1,\epsilon,(A;\lambda)} + H v_{\ell,\epsilon,(A;\lambda)} + \frac{i\tau}{2} e^{i\phi_{\lambda}} w_{\epsilon,(A;\lambda)} \\ \epsilon w_{\epsilon,(A;\lambda)} &= -i\tau \{e^{i\phi_{\lambda}} u_{\ell,\epsilon,(A;\lambda)} + e^{-i\phi_{\lambda}} v_{\ell,\epsilon,(A;\lambda)}\} \quad . \end{aligned} \quad (\text{C.3})$$

We look for solutions of Eqs.(C.2) of the form

$$\begin{bmatrix} u_{j,\epsilon,(A;\lambda)} \\ v_{j,\epsilon,(A;\lambda)} \end{bmatrix} = \begin{bmatrix} \alpha_{\epsilon,(A;\lambda)} e^{ikj} + \beta_{\epsilon,(A;\lambda)} e^{-ikj} \\ \gamma_{\epsilon,(A;\lambda)} e^{-ik'j} + \delta_{\epsilon,(A;\lambda)} e^{ik'j} \end{bmatrix} \quad , \quad (\text{C.4})$$

with $\epsilon = -2J \cos(k) - H = 2J \cos(k') + H$ and $\alpha_{\epsilon,(A;\lambda)}, \beta_{\epsilon,(A;\lambda)}, \gamma_{\epsilon,(A;\lambda)}, \delta_{\epsilon,(A;\lambda)}$ amplitudes independent of j . On inserting Eqs.(C.4) into Eqs.(C.3) and on getting rid of $w_{\epsilon,(A;\lambda)}$, we eventually obtain

$$\begin{aligned} 0 &= J u_{\ell+1,\epsilon,(A;\lambda)} + \frac{\tau^2}{2\epsilon} \{u_{\ell,\epsilon,(A;\lambda)} + e^{-2i\phi_{\lambda}} v_{\ell,\epsilon,(A;\lambda)}\} \\ 0 &= -J v_{\ell+1,\epsilon,(A;\lambda)} + \frac{\tau^2}{2\epsilon} \{e^{2i\phi_{\lambda}} u_{\ell,\epsilon,(A;\lambda)} + v_{\ell,\epsilon,(A;\lambda)}\} \quad . \end{aligned} \quad (\text{C.5})$$

In the low-energy, long-wavelength limit, Eqs.(C.5) imply $u_{\ell,\epsilon,(A;\lambda)} + e^{-2i\phi_{\lambda}} v_{\ell,\epsilon,(A;\lambda)} = 0$. To recover the low-energy description about the Fermi point k_F defined by $-2J \cos(k_F) - H = 0$, we set $k \approx k_F + \frac{\epsilon}{v}$, and $k' \approx k_F - \frac{\epsilon}{v}$, with $v = 2J \sin(k_F)$. Accordingly, Eq.(C.4) becomes

$$\begin{bmatrix} u_{j,\epsilon,(A;\lambda)} \\ v_{j,\epsilon,(A;\lambda)} \end{bmatrix} \approx \begin{bmatrix} \alpha_{(A;\lambda);\epsilon} e^{ik_F j} e^{i\frac{\epsilon x_j}{v}} + \beta_{(A;\lambda);\epsilon} e^{-ik_F j} e^{-i\frac{\epsilon x_j}{v}} \\ \gamma_{(A;\lambda);\epsilon} e^{-ik_F j} e^{i\frac{\epsilon x_j}{v}} + \delta_{(A;\lambda);\epsilon} e^{ik_F j} e^{-i\frac{\epsilon x_j}{v}} \end{bmatrix} \quad , \quad (\text{C.6})$$

with $x_j = aj$, a being the lattice step, while Eqs.(C.5) are equivalent to the condition

$$e^{i\phi_{\lambda}} \{e^{ik_F \ell} \alpha_{(A;\lambda);\epsilon} e^{i\frac{\epsilon \ell}{v}} + e^{-ik_F \ell} \beta_{(A;\lambda);\epsilon} e^{-i\frac{\epsilon \ell}{v}}\} + e^{-i\phi_{\lambda}} \{e^{-ik_F \ell} \gamma_{(A;\lambda);\epsilon} e^{i\frac{\epsilon \ell}{v}} + e^{ik_F \ell} \delta_{(A;\lambda);\epsilon} e^{-i\frac{\epsilon \ell}{v}}\} = 0 \quad . \quad (\text{C.7})$$

Inverting Eq.(C.1) and using Eqs.(C.6), we obtain the low-energy, long-wavelength mode expansion for the lattice field operator in the Heisenberg representation at time t , $c_{j,\lambda}(t)$, which is given by

$$c_{j,\lambda}(t) \approx e^{ik_F j} \psi_{R,\lambda}(x_j - vt) + e^{-ik_F j} \psi_{L,\lambda}(-x_j - vt) \quad , \quad (\text{C.8})$$

with

$$\begin{aligned} \psi_{R,\lambda}(x - vt) &= \sum_A \sum_{\epsilon} \{ \alpha_{(A;\lambda);\epsilon} \Gamma_{\epsilon;A} + [\gamma_{(A;\lambda);\epsilon}]^* \Gamma_{-\epsilon;A}^\dagger \} e^{i\frac{\epsilon}{v}(x-vt)} \\ \psi_{L,\lambda}(-x - vt) &= \sum_A \sum_{\epsilon} \{ \beta_{(A;\lambda);\epsilon} \Gamma_{\epsilon;A} + [\delta_{(A;\lambda);\epsilon}]^* \Gamma_{-\epsilon;A}^\dagger \} e^{-i\frac{\epsilon}{v}(x+vt)} \quad . \end{aligned} \quad (\text{C.9})$$

Furthermore, from Eqs.(C.7) we find that the chiral fields $\psi_{R,\lambda}, \psi_{L,\lambda}$ can be expressed in terms of a single, chiral field ψ_λ , such that

$$\begin{aligned} \psi_{R,\lambda}(x - vt) &= e^{-i\phi_\lambda} \psi_\lambda(x_j - \ell - vt) \\ \psi_{L,\lambda}(x + vt) &= -e^{-i\phi_\lambda} \psi_\lambda^\dagger(-x_j + \ell - vt) \quad . \end{aligned} \quad (\text{C.10})$$

Eq.(C.10) is independent of the boundary conditions at the inner boundaries of the chains. Once these are defined, as well, they induce further constraints among the fields $\psi_\lambda, \psi_\lambda^\dagger$. For instance, choosing open boundary conditions at the inner boundary, that is, setting $c_{j=0,\lambda} = 0$, $\forall \lambda = 1, \dots, N$ (which corresponds to the disconnected junction limit, $J_\Delta = 0$), we recover the corresponding boundary conditions on the BDG wavefunctions, given by $u_{j=0,\epsilon,(A;\lambda)} = v_{j=0,\epsilon,(A;\lambda)} = 0$. Combining these conditions with the general result of Eqs.(C.7), we readily find as many independent solutions of the BDG equations at each allowed value of ϵ , as many chains, each solution being nonzero over a single chain only. In particular, the solution being nonzero over chain- λ only is given by

$$\begin{bmatrix} u_{j;\epsilon;\lambda} \\ v_{j;\epsilon;\lambda} \end{bmatrix} = \begin{bmatrix} e^{-i\phi_\lambda} \{ \alpha_{\lambda;\epsilon} e^{ik_F j} e^{i\frac{\epsilon}{v}(x_j-\ell)} + \beta_{\lambda;\epsilon} e^{-ik_F j} e^{-i\frac{\epsilon}{v}(x_j-\ell)} \} \\ -e^{i\phi_\lambda} \{ \alpha_{\lambda;\epsilon} e^{ik_F j} e^{-i\frac{\epsilon}{v}(x_j-\ell)} + \beta_{\lambda;\epsilon} e^{-ik_F j} e^{i\frac{\epsilon}{v}(x_j-\ell)} \} \end{bmatrix} \quad , \quad (\text{C.11})$$

with $\alpha_{\lambda;\epsilon}, \beta_{\lambda;\epsilon}$ constants.

The boundary conditions at the inner boundary imply

$$\begin{aligned} \alpha_{\lambda;\epsilon} e^{-i\frac{\epsilon}{v}\ell} + \beta_{\lambda;\epsilon} e^{i\frac{\epsilon}{v}\ell} &= 0 \\ \alpha_{\lambda;\epsilon} e^{i\frac{\epsilon}{v}\ell} + \beta_{\lambda;\epsilon} e^{-i\frac{\epsilon}{v}\ell} &= 0 \quad , \end{aligned} \quad (\text{C.12})$$

which yields energy levels independent of ϕ_λ and the constants $(\alpha_{\lambda;\epsilon}, \beta_{\lambda;\epsilon}) \equiv (\alpha_\lambda, \beta_\lambda)$ independent of ϵ (as it must be). Accordingly, the mode expansion in Eq.(C.8) reduces to

$$\begin{aligned} c_{j,\lambda}(t) &\approx e^{ik_F j} e^{-i\phi_\lambda} \sum_{\epsilon} \{ \alpha_\lambda \Gamma_{\epsilon} + \alpha_\lambda^* \Gamma_{-\epsilon}^\dagger \} e^{i\frac{\epsilon}{v}(x_j-vt)} - e^{-ik_F j} e^{-i\phi_\lambda} \sum_{\epsilon} \{ \alpha_\lambda \Gamma_{\epsilon} + \alpha_\lambda^* \Gamma_{-\epsilon}^\dagger \} e^{-i\frac{\epsilon}{v}(x_j+vt)} \\ &\equiv e^{ik_F j} e^{-i\phi_\lambda} \xi_\lambda(x_j - vt) - e^{-ik_F j} e^{-i\phi_\lambda} \xi_\lambda(-x_j - vt) \quad , \end{aligned} \quad (\text{C.13})$$

with $\xi_\lambda(x - vt)$ being a chiral, real fermionic field, given by

$$\xi_\lambda(x - vt) = \frac{1}{\sqrt{\ell + 1}} \sum_{n=-\infty}^{\infty} \xi_{n,\lambda} e^{i\frac{\pi n}{\ell}(x-vt)} \quad , \quad (\text{C.14})$$

with $\xi_{n,\lambda} = \xi_{-n,\lambda}^\dagger$ and $\{\xi_{n,\lambda}, \xi_{n',\lambda'}\} = 2\delta_{n+n',0}\delta_{\lambda,\lambda'}$. Eq.(C.14) is what we have used in the main text in the disconnected junction limit.

Appendix D. Fermion parity and state counting in real fermion Hamiltonians

In this Appendix we show how to count the eigenstates of the projected boundary Hamiltonian $H_{\Delta;0}^{(3)}$ in Eq.(25) of the main text. To do so, we review and pertinently adapt to our system the approach originally developed in Ref.[54] to account for the total fermion parity conservation in a system described by a three real fermion Hamiltonian.

Following Ref.[54], we start by considering an Hamiltonian H_{Real} given by

$$H_{\text{Real}} = -ib_1\gamma_2\gamma_3 - ib_2\gamma_3\gamma_1 - ib_3\gamma_1\gamma_2 \quad , \quad (\text{D.1})$$

with b_1, b_2, b_3 real parameters. In order to pertinently take into account the fermion parity conservation, in Ref.[54], it has been proposed to realize the Majorana fermion operators as

$$\begin{aligned} \gamma_1 &\rightarrow \sigma^x \otimes \mathbf{I} = \begin{bmatrix} \sigma^x & \mathbf{0} \\ \mathbf{0} & \sigma^x \end{bmatrix} \\ \gamma_2 &\rightarrow \sigma^z \otimes \mathbf{I} = \begin{bmatrix} \sigma^z & \mathbf{0} \\ \mathbf{0} & \sigma^z \end{bmatrix} \\ \gamma_3 &\rightarrow \sigma^y \otimes \tau^x = \begin{bmatrix} \mathbf{0} & \sigma^y \\ \sigma^y & \mathbf{0} \end{bmatrix} \quad , \end{aligned} \quad (\text{D.2})$$

with the bilinears that realize the spin-1/2 $su(2)$ -algebra given by

$$\begin{aligned} \mathcal{S}^x &= \frac{i}{2}\gamma_2\gamma_3 = \frac{1}{2} \begin{bmatrix} \mathbf{0} & \sigma^x \\ \sigma^x & \mathbf{0} \end{bmatrix} \\ \mathcal{S}^y &= \frac{i}{2}\gamma_3\gamma_1 = \frac{1}{2} \begin{bmatrix} \mathbf{0} & \sigma^z \\ \sigma^z & \mathbf{0} \end{bmatrix} \\ \mathcal{S}^z &= \frac{i}{2}\gamma_1\gamma_2 = \frac{1}{2} \begin{bmatrix} \sigma^y & \mathbf{0} \\ \mathbf{0} & \sigma^y \end{bmatrix} \quad . \end{aligned} \quad (\text{D.3})$$

The fermion parity operator P , that anticommutes with all the real fermion operators and commutes with all the bilinears, is given by

$$P = \begin{bmatrix} \sigma^y & \mathbf{0} \\ \mathbf{0} & -\sigma^y \end{bmatrix} \quad . \quad (\text{D.4})$$

with $[P, H_{\text{Real}}] = 0$. Therefore, it is possible to diagonalize, H_{Real} over subspaces of a given total fermion parity. As a well-suited parity operator, P has eigenvalues $\lambda_P = \pm 1$. The projectors on the two corresponding eigenspaces, P_{\pm} , are given by

$$P_{\pm} = \frac{1}{2} \{\mathbf{I}_4 \pm P\} = \begin{bmatrix} \frac{1}{2} \{\mathbf{I} \pm \sigma^y\} & \mathbf{0} \\ \mathbf{0} & \frac{1}{2} \{\mathbf{I} \mp \sigma^y\} \end{bmatrix} . \quad (\text{D.5})$$

In general, a (4-component) vector belonging to the eigenvalue $\lambda_P = \pm 1$ takes the form

$$\begin{bmatrix} w_1 \\ w_2 \\ w_3 \\ w_4 \end{bmatrix}_{\pm} = \frac{1}{\sqrt{2}} \begin{bmatrix} z_1 \\ iz_1 \\ iz_2 \\ z_2 \end{bmatrix}, \quad \begin{bmatrix} w_1 \\ w_2 \\ w_3 \\ w_4 \end{bmatrix}_{\mp} = \frac{1}{\sqrt{2}} \begin{bmatrix} z_1 \\ -iz_1 \\ -iz_2 \\ z_2 \end{bmatrix}, \quad (\text{D.6})$$

with $|z_1|^2 + |z_2|^2 = 1$.

Next, within each fermion parity eigenspace, we diagonalize \mathcal{S}^z . In particular, we obtain the following states

- In the $\lambda_P = +1$ -sector

$$|+\rangle_1 = \frac{1}{\sqrt{2}} \begin{bmatrix} 1 \\ i \\ 0 \\ 0 \end{bmatrix}, \quad |-\rangle_1 = \frac{1}{\sqrt{2}} \begin{bmatrix} 0 \\ 0 \\ i \\ 1 \end{bmatrix}; \quad (\text{D.7})$$

- In the $\lambda_P = -1$ -sector

$$|+\rangle_{-1} = \frac{1}{\sqrt{2}} \begin{bmatrix} 0 \\ 0 \\ -i \\ 1 \end{bmatrix}, \quad |-\rangle_{-1} = \frac{1}{\sqrt{2}} \begin{bmatrix} 1 \\ -i \\ 0 \\ 0 \end{bmatrix}. \quad (\text{D.8})$$

Clearly, in either one of the two sets of states listed above, H_{Real} acts as $-2\vec{b} \cdot \vec{S}$.

It is important to note how the two sectors with different fermion parity are mixed with each other under the action of the γ_a -operators. We obtain

$${}_1\langle \pm | \gamma_a | \pm \rangle_1 = {}_{-1}\langle \pm | \gamma_a | \pm \rangle_{-1} = 0, \quad (\text{D.9})$$

as well as (listing only the nonzero matrix elements)

$$\begin{aligned} {}_{-1}\langle \pm | \gamma_1 | \mp \rangle_1 &= -{}_1\langle \pm | \gamma_1 | \mp \rangle_{-1} = i \\ {}_{-1}\langle \pm | \gamma_2 | \mp \rangle_1 &= -{}_1\langle \pm | \gamma_2 | \mp \rangle_{-1} = 1 \\ {}_{-1}\langle \pm | \gamma_3 | \pm \rangle_1 &= -{}_1\langle \pm | \gamma_3 | \pm \rangle_{-1} = \pm i. \end{aligned} \quad (\text{D.10})$$

Eqs.(D.10) are the key results used in deriving the RG equations in Sec.5.

Naively rewriting $H_{\Delta;0}^{(3)}$ as $H_{\Delta;0}^{(3)} \rightarrow \sum_{\lambda=1}^3 G_{\lambda} \sigma_{\eta}^{\lambda} \sigma_{\Gamma}^{\lambda}$, with $\{\sigma_{\eta}^{\lambda}, \sigma_{\Gamma}^{\lambda}\}$ Pauli matrices acting onto orthogonal spaces, would yield a total of 4 independent states. However, since $H_{\Delta;0}^{(3)}$ depends on 6 independent real fermionic modes, its Hilbert space should contain 8 states in total. To fix this flaw, we resort to the construction discussed above and employ it to build two (energy degenerate) copies of each eigenstate of $H_{\Delta;0}^{(3)}$, with different eigenvalues of a properly defined fermion parity operator. Since additional contributions to $H_{\Delta}^{(3)}$ including nonzero degrees of freedom of the chains commute with the operator P_{η} measuring the total fermion parity associated to the triple $\{\eta^1, \eta^2, \eta^3\}$, as well as with the operator P_{Γ} measuring the total fermion parity associated to the triple $\{\Gamma_{0,1}, \Gamma_{0,2}, \Gamma_{0,3}\}$, we choose to label the degenerate eigenstates of $H_{\Delta;0}^{(3)}$ with the total fermion parity $\mathcal{P}_{\tau} = P_{\Gamma} \cdot P_{\eta}$. Accordingly, we choose as basis set of the space of states of $H_{\Delta;0}^{(3)}$ the 8 states $|a_{\Gamma}, a_{\eta}\rangle_{\gamma}$, such that

$$\begin{aligned} \sigma_{\Gamma}^3 |a_{\Gamma}, a_{\eta}\rangle_{\gamma} &= i\Gamma_{0,1}\Gamma_{0,2} |a_{\Gamma}, a_{\eta}\rangle_{\gamma} = a_{\Gamma} |a_{\Gamma}, a_{\eta}\rangle_{\gamma} \\ \sigma_{\eta}^3 |a_{\Gamma}, a_{\eta}\rangle_{\gamma} &= i\eta^1\eta^2 |a_{\Gamma}, a_{\eta}\rangle_{\gamma} = a_{\eta} |a_{\Gamma}, a_{\eta}\rangle_{\gamma} \\ \mathcal{P}_{\tau} |a_{\Gamma}, a_{\eta}\rangle_{\gamma} &= \gamma |a_{\Gamma}, a_{\eta}\rangle_{\gamma} \quad , \end{aligned} \quad (\text{D.11})$$

and $a_{\Gamma}, a_{\eta}, \gamma = \pm 1$.

$H_{\Delta;0}^{(3)}$ commutes with P_{τ} . Therefore, at a fixed value of γ , within the subspace spanned by the states $\{|a_{\Gamma}, a_{\eta}\rangle_{\gamma}\}$, it is represented by the 4×4 matrix $h_{3;0}$, given by

$$h_{3;0} = \begin{bmatrix} 2J_{1,2} & 0 & 0 & 2J_{2,3} - 2J_{3,1} \\ 0 & -2J_{1,2} & 2J_{2,3} + 2J_{3,1} & 0 \\ 0 & 2J_{2,3} + 2J_{3,1} & -2J_{1,2} & 0 \\ 2J_{2,3} - 2J_{3,1} & 0 & 0 & 2J_{1,2} \end{bmatrix} . \quad (\text{D.12})$$

$h_{3;0}$ can be readily diagonalized. Below we report the list of the eigenvalues ($\{\epsilon_j\}$), together with the corresponding eigenvectors ($\{|\psi_{\gamma}\rangle_j\}$), which was the starting point for the derivation of Sec.4:

$$\begin{aligned} \epsilon_1 &= -2 \{J_{1,2} + J_{2,3} + J_{3,1}\} \quad , \quad |\psi_{\gamma}\rangle_1 = \frac{1}{\sqrt{2}} \{|+, -\rangle_{\gamma} - |-, +\rangle_{\gamma}\} \\ \epsilon_2 &= -2 \{J_{1,2} - J_{2,3} - J_{3,1}\} \quad , \quad |\psi_{\gamma}\rangle_2 = \frac{1}{\sqrt{2}} \{|+, -\rangle_{\gamma} + |-, +\rangle_{\gamma}\} \\ \epsilon_3 &= 2 \{J_{1,2} + J_{2,3} - J_{3,1}\} \quad , \quad |\psi_{\gamma}\rangle_3 = \frac{1}{\sqrt{2}} \{|+, +\rangle_{\gamma} + |-, -\rangle_{\gamma}\} \\ \epsilon_4 &= 2 \{J_{1,2} - J_{2,3} + J_{3,1}\} \quad , \quad |\psi_{\gamma}\rangle_4 = \frac{1}{\sqrt{2}} \{|+, +\rangle_{\gamma} - |-, -\rangle_{\gamma}\} . \end{aligned} \quad (\text{D.13})$$

Appendix E. Explicit solution of Eqs.(37) and renormalization group trajectories

In Sec.5 we have derived the RG equations for the running couplings $G_{\lambda, \lambda+1}$. In particular, in Eqs.(36), we get the exact equations by pertinently taking into account the breaking of the system groundstate degeneracy due to the hybridization between the zero-modes of the chains. At the

same time, we stressed that, for all the practical purposes, Eqs.(36) may be substituted with the simplified Eqs.(37), which are the “standard” RG equations for the anisotropic TKE.

In this Appendix, we discuss in detail how to recover the Kondo length ℓ_K as a function of the bare couplings. This is a crucial step of all our derivation, as the dependence of ℓ_K on the $G_{\lambda,\lambda+1}^{(0)}$ s, which are known functions of the applied phases, determines how, and to what extent, the Kondo length is tuned by acting on $\Delta\phi_a, \Delta\phi_b$. For this reason, we first discuss the general case in which the bare couplings are all different from each other and in which the formula for ℓ_K as a function of the $G_{\lambda,\lambda+1}^{(0)}$ s can only approximately be recovered, and then focus onto the cases in which two of the $G_{\lambda,\lambda+1}^{(0)}$ s are equal to each other, when an exact, explicit formula for ℓ_K can be provided within the approach of Refs.[39, 32, 35].

We note that, acting on $\Delta\phi_a, \Delta\phi_b$, we can not only change the relative magnitudes of the running couplings, but also their sign. Accordingly, we have to consider all the possible sign assignments for the running couplings. To begin with, we assume that all three the $G_{\lambda,\lambda+1}$ ’s have positive sign. In this case, since Eqs.(37) yield

$$\frac{d[G_{\lambda,\lambda+1} - G_{\lambda+1,\lambda+2}]}{dl} = -G_{\lambda+2,\lambda} \{G_{\lambda,\lambda+1} - G_{\lambda+1,\lambda+2}\} \quad , \quad (\text{E.1})$$

we conclude that the difference in the initial values of the running couplings is washed out along the renormalization group trajectories and that the boundary Kondo interaction flows toward an isotropic fixed point, which we identify with the one of a Y junction of three quantum Ising chains [37, 66, 39].

To estimate ℓ_K , we note that Eqs.(37) imply that $G_{\lambda,\lambda+1}^2(l) - G_{\lambda+1,\lambda+2}^2(l)$ are constant along the renormalization group trajectories for any λ . Therefore, assuming, for instance, that $G_{1,2}^{(0)} \leq G_{2,3}^{(0)} \leq G_{3,1}^{(0)}$, we use the conservation laws to trade Eqs.(37) for an equation involving $G_{1,2}(l)$ only, that is given by

$$\frac{dG_{1,2}(l)}{dl} = \sqrt{[G_{2,3}^2(0) - G_{1,2}^2(0) + G_{1,2}^2(l)] [G_{3,1}^2(0) - G_{1,2}^2(0) + G_{1,2}^2(l)]} \quad . \quad (\text{E.2})$$

Once we have solved Eq.(E.2) for $G_{1,2}(l)$, we obtain $G_{2,3}(l) = \sqrt{G_{1,2}^2(l) + [G_{2,3}^{(0)}]^2 - [G_{1,2}^{(0)}]^2}$, and $G_{3,1}(l) = \sqrt{G_{1,2}^2(l) + [G_{3,1}^{(0)}]^2 - [G_{1,2}^{(0)}]^2}$. Therefore, the scale at which the perturbation theory breaks down can be uniquely identified as the scale at which $G_{1,2}(l)$ diverges.

Determining ℓ_K from Eq.(E.2) requires introducing the incomplete elliptic integral, so that we eventually find

$$\mathcal{F} \left(\frac{\pi}{2} \middle| 1 - \frac{[G_{3,1}^{(0)}]^2 - [G_{1,2}^{(0)}]^2}{[G_{2,3}^{(0)}]^2 - [G_{1,2}^{(0)}]^2} \right) - \arctan \left[\frac{G_{1,2}^{(0)}}{\sqrt{[G_{2,3}^{(0)}]^2 - [G_{1,2}^{(0)}]^2}} \right] \approx \sqrt{[G_{3,1}^{(0)}]^2 - [G_{1,2}^{(0)}]^2} \ln \left(\frac{\ell_K}{\ell_0} \right) \quad , \quad (\text{E.3})$$

with

$$\mathcal{F}(\omega|z) = \int_0^\omega \frac{dt}{\sqrt{1-zt^2}} \quad . \quad (\text{E.4})$$

To investigate the other possibilities, let us first of all assume, without loss of generality, that the initial couplings $G_{\lambda,\lambda+1}^{(0)}$ are such that $G_{1,2}^{(0)} \leq 0 < G_{2,3}^{(0)} \leq G_{3,1}^{(0)}$. Nothing changes with respect to the case $G_{1,2}^{(0)} > 0$, if $|G_{1,2}^{(0)}| < G_{2,3}^{(0)}$. In this case, while $G_{1,2}(l)$ start growing toward 0 as l increases, $G_{2,3}(l)$ and $G_{3,1}(l)$ decrease toward 0. $G_{1,2}(l)$ has to become 0 before $G_{2,3}(l)$ and $G_{3,1}(l)$ do so. This arises from the observation that Eqs.(37) imply that the three functions $G_{\lambda,\lambda+1}^2(l) - G_{\lambda+1,\lambda+2}^2(l)$ are all constant along the RG trajectories. If there was a scale \hat{l} at which $G_{2,3}(\hat{l}) = 0$ and, at the same time, $G_{1,2}(\hat{l}) \neq 0$, then one would get $G_{2,3}^2(\hat{l}) - G_{1,2}^2(\hat{l}) = -G_{1,2}^2(\hat{l}) < 0$, which apparently contradicts the fact that $G_{2,3}^2(\hat{l}) - G_{1,2}^2(l) = [G_{2,3}^{(0)}]^2 - [G_{1,2}^{(0)}]^2 > 0$ at any scale l . Beyond \hat{l} , the RG trajectories are the same as in the case $G_{1,2}^{(0)} > 0$ and ℓ_K can be again estimated exactly as in Eq.(E.3), by just substituting $G_{\lambda,\lambda+1}^{(0)}$ with $G_{\lambda,\lambda+1}(\hat{l})$ and ℓ_0 with $\ln(\hat{l})$.

At variance, when $|G_{1,2}^{(0)}| > G_{2,3}^{(0)}$, $G_{2,3}(l)$ becomes 0 at a scale \bar{l} at which we still have $G_{1,2}(\bar{l}) < 0$, which is a consequence of the fact that now the constant of motion is $[G_{2,3}^{(0)}]^2 - [G_{1,2}^{(0)}]^2 < 0$. At scales $l > \bar{l}$, both $G_{1,2}(l)$ and $G_{2,3}(l)$ grow large and negative, while $G_{3,1}(l)$ grows large and positive. In addition, from Eqs.(37) we readily derive that, at scales $l > \bar{l}$, $|G_{\lambda,\lambda+1}(l)| - |G_{\lambda+1,\lambda+2}(l)|$ renormalizes to 0, according to

$$\frac{d[|G_{\lambda,\lambda+1}(l)| - |G_{\lambda+1,\lambda+2}(l)|]}{dl} = -|G_{\lambda+2,\lambda}(l)| \{|G_{\lambda,\lambda+1}(l)| - |G_{\lambda+1,\lambda+2}(l)|\} \quad . \quad (\text{E.5})$$

Thus, we infer that the strongly coupled fixed point, in this case, corresponds to $G_{1,2}(l), G_{2,3}(l) \rightarrow -\infty$; $G_{3,1}(l) \rightarrow +\infty$, as $l \rightarrow \infty$, with $(|G_{\lambda,\lambda+1}(l)|/|G_{\lambda',\lambda'+1}(l)|) \rightarrow 1$. In fact, this is equivalent to the isotropic strongly coupled fixed point to which the system flows when all the boundary couplings are > 0 , up to the replacement $\eta_2 \rightarrow -\eta_2$. Finally, we note that the same argument applies equally well to the case in which $|G_{1,2}^{(0)}| > G_{3,1}^{(0)} \geq G_{2,3}^{(0)}$, so, the same conclusions hold in this latter case, as well. In this case, ℓ_K is estimated as above, by just using $\ell_0 = \ln(\bar{l})$ as the reference scale.

The above conclusions apply, as well, to the case $G_{1,2}^{(0)} < G_{2,3}^{(0)} < 0 < G_{3,1}^{(0)}$, except that now we have to set $\bar{l} = 0$. Finally, in the case $G_{1,2}^{(0)} \leq G_{2,3}^{(0)} \leq G_{3,1}^{(0)} < 0$, all the β -functions at the right-hand side of Eqs.(37) are > 0 and, accordingly, all the running couplings start their flow by increasing toward 0, that is, by decreasing their absolute values. At a scale \bar{l} , $G_{3,1}(\bar{l}) = 0$. Similar arguments to the ones used above imply $G_{1,2}(\bar{l}) < 0, G_{2,3}(\bar{l}) < 0$. Thus, being $\beta_{3,1}[G_{1,2}(\bar{l}), G_{2,3}(\bar{l}), G_{3,1}(\bar{l})] > 0$, $G_{3,1}(l)$ becomes positive at scales $l > \bar{l}$. Accordingly, we again obtain that the strongly coupled fixed point corresponds to $G_{1,2}(l), G_{2,3}(l) \rightarrow -\infty$; $G_{3,1}(l) \rightarrow +\infty$, as $l \rightarrow \infty$, with $(|G_{\lambda,\lambda+1}(l)|/|G_{\lambda',\lambda'+1}(l)|) \rightarrow 1$. ℓ_K in this case can be estimated accordingly. To summarize the results obtained above, we conclude that, if the bare couplings are all different from each other, regardless of their relative sign, the junction always flows toward the Kondo fixed point.

Note that from the above discussion we left aside the ‘‘critical lines’’ $|G_{1,2}^{(0)}| = G_{2,3}^{(0)}$ and $|G_{1,2}^{(0)}| = G_{3,1}^{(0)}$, as well as the partially isotropic cases (when all the three couplings are positive) $G_{1,2}^{(0)} = G_{2,3}^{(0)}$ and $G_{1,2}^{(0)} = G_{3,1}^{(0)}$. In this special cases it is possible to provide simple, closed-form analytical formulas for the running couplings, which we discuss in the following.

To begin with, let us consider the region in which all three the couplings are > 0 and let us assume that, without loss of generality, $G_{1,2}^{(0)} = G_{2,3}^{(0)}$. The corresponding RG equations are therefore a simplified version of the one discussed in, e.g., Ref.[35] for an impurity embedded within a

quantum XXZ spin chain. Indeed, being $G_{1,2}^2(l) - G_{2,3}^2(l)$ constant along the RG trajectories, we find that $G_{1,2}(l) = G_{2,3}(l)$ at any scale l , which allows for simplifying Eqs.(37) to

$$\begin{aligned}\frac{dG_{1,2}}{dl} &= G_{1,2}G_{3,1} \\ \frac{dG_{3,1}}{dl} &= G_{1,2}^2 \quad .\end{aligned}\tag{E.6}$$

Depending on the relative values of $G_{1,2}^{(0)}$ and of $G_{3,1}^{(0)}$, we therefore obtain the following explicit solutions (listed together with the corresponding estimate of ℓ_K)

- $G_{1,2}^{(0)} = G_{2,3}^{(0)} > G_{3,1}^{(0)}$

In this case we obtain [35]

$$\begin{aligned}G_{3,1}\left[l = \left(\frac{\ell}{\ell_0}\right)\right] &= \sqrt{[G_{1,2}^{(0)}]^2 - [G_{3,1}^{(0)}]^2} \tan \left\{ \arctan \left[\frac{G_{3,1}^{(0)}}{\sqrt{[G_{1,2}^{(0)}]^2 - [G_{3,1}^{(0)}]^2}} \right] + \sqrt{[G_{1,2}^{(0)}]^2 - [G_{3,1}^{(0)}]^2} \ln \left(\frac{\ell}{\ell_0} \right) \right\} \\ G_{1,2}\left[l = \left(\frac{\ell}{\ell_0}\right)\right] &= \sqrt{[G_{1,2}^{(0)}]^2 - [G_{3,1}^{(0)}]^2 + G_{3,1}^2\left[l = \left(\frac{\ell}{\ell_0}\right)\right]} \quad ,\end{aligned}\tag{E.7}$$

which implies

$$\sqrt{[G_{1,2}^{(0)}]^2 - [G_{3,1}^{(0)}]^2} \ln \left(\frac{\ell_K}{\ell_0} \right) = \frac{\pi}{2} - \arctan \left[\frac{G_{3,1}^{(0)}}{\sqrt{[G_{1,2}^{(0)}]^2 - [G_{3,1}^{(0)}]^2}} \right] \quad ,\tag{E.8}$$

in perfect agreement with Eq.(E.3).

- $G_{1,2}^{(0)} = G_{2,3}^{(0)} < G_{3,1}^{(0)}$

In this case we obtain

$$\begin{aligned}G_{3,1}\left[l = \left(\frac{\ell}{\ell_0}\right)\right] &= \sqrt{[G_{3,1}^{(0)}]^2 - [G_{1,2}^{(0)}]^2} \times \\ &\quad \left\{ \frac{G_{3,1}^{(0)} + \sqrt{[G_{3,1}^{(0)}]^2 - [G_{1,2}^{(0)}]^2} + [G_{3,1}^{(0)} - \sqrt{[G_{3,1}^{(0)}]^2 - [G_{1,2}^{(0)}]^2}] \left(\frac{\ell}{\ell_0}\right)^2 \sqrt{[G_{3,1}^{(0)}]^2 - [G_{1,2}^{(0)}]^2}}{G_{3,1}^{(0)} + \sqrt{[G_{3,1}^{(0)}]^2 - [G_{1,2}^{(0)}]^2} - [G_{3,1}^{(0)} - \sqrt{[G_{3,1}^{(0)}]^2 - [G_{1,2}^{(0)}]^2}] \left(\frac{\ell}{\ell_0}\right)^2 \sqrt{[G_{3,1}^{(0)}]^2 - [G_{1,2}^{(0)}]^2}} \right\} \\ G_{1,2}\left[l = \left(\frac{\ell}{\ell_0}\right)\right] &= \sqrt{[G_{1,2}^{(0)}]^2 - [G_{3,1}^{(0)}]^2 + G_{3,1}^2\left[l = \left(\frac{\ell}{\ell_0}\right)\right]} \quad ,\end{aligned}\tag{E.9}$$

which yields [39]

$$\ell_K = \ell_0 \left\{ \frac{G_{3,1}^{(0)} + \sqrt{[G_{3,1}^{(0)}]^2 - [G_{1,2}^{(0)}]^2}}{G_{3,1}^{(0)} - \sqrt{[G_{3,1}^{(0)}]^2 - [G_{1,2}^{(0)}]^2}} \right\}^{\frac{1}{2\sqrt{[G_{3,1}^{(0)}]^2 - [G_{1,2}^{(0)}]^2}}}, \quad (\text{E.10})$$

that can again be recovered from Eq.(E.3) by going through an appropriate analytical continuation of the functions involved.

- $G_{1,2}^{(0)} = G_{2,3}^{(0)} = G_{3,1}^{(0)}$

Finally, in the fully isotropic case, we obtain back the renormalization group equations for the standard, isotropic Kondo effect, which is solved by

$$G_{1,2} \left[l = \left(\frac{\ell}{\ell_0} \right) \right] = \frac{G_{1,2}^{(0)}}{1 - G_{1,2}^{(0)} \ln \left(\frac{\ell}{\ell_0} \right)}, \quad (\text{E.11})$$

implying

$$\ell_K = \ell_0 \exp \left[\frac{1}{G_{1,2}^{(0)}} \right], \quad (\text{E.12})$$

that is, the well-celebrated formula for the Kondo length in the isotropic case [2].

- $G_{3,1}^{(0)} < 0 < G_{1,2}^{(0)} = G_{2,3}^{(0)}, |G_{3,1}^{(0)}| < G_{1,2}^{(0)}$

In this case the solution for the running couplings takes the same form as in Eq.(E.7), while ℓ_K is again given by Eq.(E.8).

- $G_{3,1}^{(0)} < 0 < G_{1,2}^{(0)} = G_{2,3}^{(0)}, |G_{3,1}^{(0)}| > G_{1,2}^{(0)}$

For this specific set of values of the “bare” parameters the solution of the RG equations is again given by Eqs.(E.9), except that now $G_{3,1}^{(0)}$ is negative, which implies

$$G_{3,1} \left[l = \left(\frac{\ell}{\ell_0} \right) \right] = \sqrt{[G_{3,1}^{(0)}]^2 - [G_{1,2}^{(0)}]^2} \times \left\{ \frac{-|G_{3,1}^{(0)}| + \sqrt{[G_{3,1}^{(0)}]^2 - [G_{1,2}^{(0)}]^2} - [|G_{3,1}^{(0)}| + \sqrt{[G_{3,1}^{(0)}]^2 - [G_{1,2}^{(0)}]^2}] \left(\frac{\ell}{\ell_0} \right)^{2\sqrt{[G_{3,1}^{(0)}]^2 - [G_{1,2}^{(0)}]^2}}}{-|G_{3,1}^{(0)}| + \sqrt{[G_{3,1}^{(0)}]^2 - [G_{1,2}^{(0)}]^2} + [|G_{3,1}^{(0)}| + \sqrt{[G_{3,1}^{(0)}]^2 - [G_{1,2}^{(0)}]^2}] \left(\frac{\ell}{\ell_0} \right)^{2\sqrt{[G_{3,1}^{(0)}]^2 - [G_{1,2}^{(0)}]^2}}} \right\}$$

$$G_{1,2} \left[l = \left(\frac{\ell}{\ell_0} \right) \right] = \sqrt{[G_{1,2}^{(0)}]^2 - [G_{3,1}^{(0)}]^2 + G_{3,1}^2 \left[l = \left(\frac{\ell}{\ell_0} \right) \right]}. \quad (\text{E.13})$$

Apparently, the solutions at the right-hand side of Eqs.(E.13) exhibit no divergences anymore. Therefore, the interaction keeps perturbative at any scale and, as $\ell \rightarrow \infty$, we eventually get

$$\begin{aligned}\lim_{\ell \rightarrow \infty} G_{3,1} \left[l = \left(\frac{\ell}{\ell_0} \right) \right] &= -\sqrt{[G_{3,1}^{(0)}]^2 - [G_{1,2}^{(0)}]^2} \\ \lim_{\ell \rightarrow \infty} G_{1,2} \left[l = \left(\frac{\ell}{\ell_0} \right) \right] &= 0 \quad .\end{aligned}\tag{E.14}$$

The RG flow in Eqs.(E.13,E.14) corresponds to what happens in the region of irrelevance of the boundary interaction describing a spin impurity embedded within a quantum XXZ spin chain [32, 35]. The crucial point is that, in order for us to have an effectively irrelevant boundary interaction, we have to fine-tune the coupling strength so that $G_{1,2}^{(0)} = G_{2,3}^{(0)}$. Would the fine-tuning condition not be satisfied, we would get back to the flow toward the strongly interacting Kondo fixed point, as discussed above.

- $G_{1,2}^{(0)} < 0 < G_{2,3}^{(0)}, |G_{1,2}^{(0)}| = G_{2,3}^{(0)}, G_{2,3}^{(0)} > G_{3,1}^{(0)} > 0$

In this case, Eqs.(37) reduce to

$$\begin{aligned}\frac{dG_{1,2}}{dl} &= -G_{1,2}G_{3,1} \\ \frac{dG_{3,1}}{dl} &= -G_{1,2}^2 \quad .\end{aligned}\tag{E.15}$$

The solution now takes the form

$$\begin{aligned}G_{3,1} \left[l = \left(\frac{\ell}{\ell_0} \right) \right] &= \sqrt{[G_{1,2}^{(0)}]^2 - [G_{3,1}^{(0)}]^2} \tan \left\{ \arctan \left[\frac{G_{3,1}^{(0)}}{\sqrt{[G_{1,2}^{(0)}]^2 - [G_{3,1}^{(0)}]^2}} \right] - \sqrt{[G_{1,2}^{(0)}]^2 - [G_{3,1}^{(0)}]^2} \ln \left(\frac{\ell}{\ell_0} \right) \right\} \\ G_{1,2} \left[l = \left(\frac{\ell}{\ell_0} \right) \right] &= -\sqrt{[G_{1,2}^{(0)}]^2 - [G_{3,1}^{(0)}]^2} + G_{3,1}^2 \left[l = \left(\frac{\ell}{\ell_0} \right) \right] \quad .\end{aligned}\tag{E.16}$$

At the scale $\hat{\ell}$ such that $\arctan \left[\frac{G_{3,1}^{(0)}}{\sqrt{[G_{1,2}^{(0)}]^2 - [G_{3,1}^{(0)}]^2}} \right] - \sqrt{[G_{1,2}^{(0)}]^2 - [G_{3,1}^{(0)}]^2} \ln \left(\frac{\hat{\ell}}{\ell_0} \right) = 0$, $G_{3,1} \left[l = \left(\frac{\ell}{\ell_0} \right) \right]$ becomes negative. At larger scales, the perturbative approach breaks down at $\ell = \ell_K$, with

$$\sqrt{[G_{1,2}^{(0)}]^2 - [G_{3,1}^{(0)}]^2} \ln \left(\frac{\ell_K}{\ell_0} \right) = \frac{\pi}{2} + \arctan \left[\frac{G_{3,1}^{(0)}}{\sqrt{[G_{1,2}^{(0)}]^2 - [G_{3,1}^{(0)}]^2}} \right] \quad .\tag{E.17}$$

- $G_{1,2}^{(0)} < 0 < G_{2,3}^{(0)}, |G_{1,2}^{(0)}| = G_{2,3}^{(0)}, 0 < G_{2,3}^{(0)} < G_{3,1}^{(0)}$

Pertinently modifying the result of Eq.(E.9), we obtain

$$\begin{aligned}
G_{3,1} \left[l = \left(\frac{\ell}{\ell_0} \right) \right] &= \sqrt{[G_{3,1}^{(0)}]^2 - [G_{1,2}^{(0)}]^2} \times \\
&\quad \left\{ \frac{G_{3,1}^{(0)} + \sqrt{[G_{3,1}^{(0)}]^2 - [G_{1,2}^{(0)}]^2} + [G_{3,1}^{(0)} - \sqrt{[G_{3,1}^{(0)}]^2 - [G_{1,2}^{(0)}]^2}] \left(\frac{\ell}{\ell_0} \right)^{-2 \sqrt{[G_{3,1}^{(0)}]^2 - [G_{1,2}^{(0)}]^2}}}{G_{3,1}^{(0)} + \sqrt{[G_{3,1}^{(0)}]^2 - [G_{1,2}^{(0)}]^2} - [G_{3,1}^{(0)} - \sqrt{[G_{3,1}^{(0)}]^2 - [G_{1,2}^{(0)}]^2}] \left(\frac{\ell}{\ell_0} \right)^{-2 \sqrt{[G_{3,1}^{(0)}]^2 - [G_{1,2}^{(0)}]^2}}} \right\} \\
G_{1,2} \left[l = \left(\frac{\ell}{\ell_0} \right) \right] &= \sqrt{[G_{1,2}^{(0)}]^2 - [G_{3,1}^{(0)}]^2} + G_{3,1} \left[l = \left(\frac{\ell}{\ell_0} \right) \right] , \tag{E.18}
\end{aligned}$$

which yields

$$\begin{aligned}
\lim_{\ell \rightarrow \infty} G_{3,1} \left[l = \left(\frac{\ell}{\ell_0} \right) \right] &= \sqrt{[G_{3,1}^{(0)}]^2 - [G_{1,2}^{(0)}]^2} \\
\lim_{\ell \rightarrow \infty} G_{1,2} \left[l = \left(\frac{\ell}{\ell_0} \right) \right] &= 0 , \tag{E.19}
\end{aligned}$$

that is, again the system flows toward the region of irrelevance of the boundary interaction describing a spin impurity embedded within a quantum XXZ spin chain [32, 35].

- $G_{3,1}^{(0)} = G_{1,2}^{(0)} = G_{2,3}^{(0)} < 0$

In this case, the RG flow corresponds to the (irrelevant) ferromagnetic Kondo interaction. Indeed, solving the renormalization group equation, we find $G_{1,2}(l) = G_{2,3}(l) = G_{3,1}(l)$, with

$$G_{1,2} \left[l = \left(\frac{\ell}{\ell_0} \right) \right] = - \frac{|G_{1,2}^{(0)}|}{1 + |G_{1,2}^{(0)}| \ln \left(\frac{\ell}{\ell_0} \right)} , \tag{E.20}$$

that implies

$$\lim_{\ell \rightarrow \infty} G_{1,2} \left[l = \left(\frac{\ell}{\ell_0} \right) \right] = 0 . \tag{E.21}$$

To synoptically summarize the results we derived in this Appendix, below we list all the fixed points to which the $N = 3$ junction flows, for any possible choice of the initial values of the couplings (up to trivial exchanges in the indices)

- **Case 1:** $G_{\lambda,\lambda+1}^{(0)} > 0 \forall \lambda$ (including the case in which one of the $G_{\lambda,\lambda+1}^{(0)} = 0$).

In this case the boundary interaction flows towards the fixed point describing the anisotropic TKE. All the running couplings flow to $+\infty$ as $\ell > \ell_K$. Nothing substantially changes if one of the bare couplings is $= 0$.

- **Case 2:** $G_{1,2}^{(0)} < 0 < G_{2,3}^{(0)} < G_{3,1}^{(0)}$.

If $|G_{1,2}^{(0)}| \leq G_{2,3}^{(0)}$, then $G_{1,2}(l)$ crosses 0 at a scale \bar{l} at which $0 < G_{2,3}(\bar{l}) < G_{3,1}(\bar{l})$. For $l > \bar{l}$ the flow is the same as in the case $G_{1,2}^{(0)} = 0 < G_{2,3}^{(0)} < G_{3,1}^{(0)}$, with all the running couplings flowing to $+\infty$.

At variance, if $|G_{1,2}^{(0)}| > G_{2,3}^{(0)}$, the system flows toward a strongly coupled fixed point with $G_{1,2}(l), G_{2,3}(l) \rightarrow -\infty$ and $G_{3,1}(l) \rightarrow +\infty$, which is equivalent to the one discussed at Case 1, provided $\eta_2 \rightarrow -\eta_2$ in the boundary Hamiltonian.

Case 2 is trivially equivalent to the case $G_{1,2}^{(0)} < 0 < G_{3,1}^{(0)} < G_{2,3}^{(0)}$, provided $G_{2,3}(l)$ and $G_{3,1}(l)$ are exchanged with each other in the discussion.

- **Case 3:** $G_{1,2}^{(0)} < 0 < G_{2,3}^{(0)} = G_{3,1}^{(0)}$.

Also in this case, for $|G_{1,2}^{(0)}| \leq G_{2,3}^{(0)}$, all the running couplings flow to $+\infty$ as $l > \ell_K$. At variance, for $|G_{1,2}^{(0)}| > G_{2,3}^{(0)}$, the system flows towards the “trivial” fixed point corresponding to Eqs.(E.19).

- **Case 4:** $G_{1,2}^{(0)} \leq G_{2,3}^{(0)} < 0 < G_{3,1}^{(0)}$.

Employing the substitutions $\eta_2 \rightarrow -\eta_2$ and $G_{1,2} \rightarrow -G_{1,2}$, $G_{2,3} \rightarrow -G_{2,3}$, this case is mapped onto Case 1, with all three the $G_{\lambda,\lambda+1}^{(0)} > 0$. Thus, we conclude that, in this case, $G_{1,2}(l), G_{2,3}(l) \rightarrow -\infty$ and $G_{3,1}(l) \rightarrow +\infty$. Exactly as in the case 1, nothing changes if either $G_{2,3}^{(0)} = 0$, or $G_{3,1}^{(0)} = 0$.

- **Case 5:** $G_{1,2}^{(0)} < G_{2,3}^{(0)} < G_{3,1}^{(0)} \leq 0$.

Using again the substitutions $\eta_2 \rightarrow -\eta_2$ and $G_{1,2} \rightarrow -G_{1,2}$, $G_{2,3} \rightarrow -G_{2,3}$, this case becomes equivalent to case 2. Thus, we conclude that, also in this case, $G_{1,2}(l), G_{2,3}(l) \rightarrow -\infty$ and $G_{3,1}(l) \rightarrow +\infty$.

- **Case 6:** $G_{1,2}^{(0)} = G_{2,3}^{(0)} < G_{3,1}^{(0)} \leq 0$.

Employing again the equivalence with case 3, we find that, also in this case, $G_{1,2}(l) = G_{2,3}(l) \rightarrow -\infty$ and $G_{3,1}(l) \rightarrow +\infty$.

- **Case 7:** $G_{1,2}^{(0)} < G_{2,3}^{(0)} = G_{3,1}^{(0)} < 0$.

In this case the system flows towards the “trivial” fixed point corresponding to Eqs.(E.19).

- **Case 8:** $G_{1,2}^{(0)} = G_{2,3}^{(0)} = G_{3,1}^{(0)} < 0$.

In this case the fixed point is a limiting case of the one corresponding to Eqs.(E.19) in which all the running couplings flow to 0.

References

- [1] J. Kondo, Progress of Theoretical Physics **32**, 37 (1964).
 [2] A. C. Hewson, The Kondo Effect to Heavy Fermions (Cambridge University Press, 1993).

- [3] L. P. Kouwenhoven and L. Glazman, *Physics World* **14**, 33 (2001).
- [4] P. Nozières, *Journal of Low Temperature Physics* **17**, 31742 (1974).
- [5] P. Nozières, *J. Phys. France* **39**, 1117 (1978).
- [6] A. W. Ludwig and I. Affleck, *Nuclear Physics B* **428**, 545 (1994).
- [7] I. Affleck and A. W. Ludwig, *Nuclear Physics B* **360**, 641 (1991).
- [8] R. Bulla, T. A. Costi, and T. Pruschke, *Rev. Mod. Phys.* **80**, 395 (2008).
- [9] A. Alivisatos, *Science* **271**, 933 (1996).
- [10] L. P. Kouwenhoven and C. Marcus, *Physics World* **11**, 35 (1998).
- [11] D. Goldhaber-Gordon, H. Shtrikman, D. Mahalu, D. Abusch-Magder, U. Meirav, and M. A. Kastner, *Nature* **391**, 156 (1998).
- [12] S. M. Cronenwett, T. H. Oosterkamp, and L. P. Kouwenhoven, *Science* **281**, 540 (1998).
- [13] D. Giuliano, L. Lepori, and A. Nava, *Phys. Rev. B* **101**, 195140 (2020).
- [14] Y. Avishai, A. Golub, and A. D. Zaikin, *Phys. Rev. B* **63**, 134515 (2001).
- [15] M.-S. Choi, M. Lee, K. Kang, and W. Belzig, *Phys. Rev. B* **70**, 020502 (2004).
- [16] G. Campagnano, D. Giuliano, A. Naddeo, and A. Tagliacozzo, *Physica C: Superconductivity* **406**, 1 (2004).
- [17] B. Béri and N. R. Cooper, *Phys. Rev. Lett.* **109**, 156803 (2012).
- [18] A. Altland, B. Béri, R. Egger, and A. M. Tsvelik, *Phys. Rev. Lett.* **113**, 076401 (2014).
- [19] F. Bucchieri, H. Babujian, V. E. Korepin, P. Sodano, and A. Trombettoni, *Nuclear Physics B* **896**, 52 (2015).
- [20] E. Eriksson, A. Nava, C. Mora, and R. Egger, *Phys. Rev. B* **90**, 245417 (2014).
- [21] K. G. Wilson, *Rev. Mod. Phys.* **47**, 773 (1975).
- [22] I. Affleck and D. Giuliano, *Journal of Statistical Physics* **157**, 666 (2014).
- [23] I. Affleck, in *Perspectives of Mesoscopic Physics* (World Scientific, Singapore, 2010), pp. 1–44.
- [24] S. Eggert and I. Affleck, *Phys. Rev. B* **46**, 10866 (1992).
- [25] A. Furusaki and T. Hikihara, *Phys. Rev. B* **58**, 5529 (1998).
- [26] N. Laflorencie, E. S. Sørensen, and I. Affleck, *Journal of Statistical Mechanics: Theory and Experiment* **2008**, P02007 (2008).
- [27] J. Sirker, S. Fujimoto, N. Laflorencie, S. Eggert, and I. Affleck, *Journal of Statistical Mechanics: Theory and Experiment* **2008**, P02015 (2008).
- [28] A. Bayat, P. Sodano, and S. Bose, *Phys. Rev. B* **81**, 064429 (2010).
- [29] A. Bayat, S. Bose, P. Sodano, and H. Johannesson, *Phys. Rev. Lett.* **109**, 066403 (2012).
- [30] L.-M. Duan, E. Demler, and M. D. Lukin, *Phys. Rev. Lett.* **91**, 090402 (2003).
- [31] D. Giuliano, D. Rossini, P. Sodano, and A. Trombettoni, *Phys. Rev. B* **87**, 035104 (2013).
- [32] D. Giuliano, P. Sodano, and A. Trombettoni, *Phys. Rev. A* **96**, 033603 (2017).
- [33] D. Giuliano and P. Sodano, *Nuclear Physics B* **711**, 480 (2005).
- [34] D. Giuliano and P. Sodano, *EPL (Europhysics Letters)* **103**, 57006 (2013).
- [35] D. Giuliano, D. Rossini, and A. Trombettoni, *Phys. Rev. B* **98**, 235164 (2018).
- [36] N. Crampé and A. Trombettoni, *Nuclear Physics B* **871**, 526 (2013).
- [37] A. M. Tsvelik, *Phys. Rev. Lett.* **110**, 147202 (2013).
- [38] D. Giuliano, G. Campagnano, and A. Tagliacozzo, *The European Physical Journal B* **89**, 251 (2016).
- [39] D. Giuliano, P. Sodano, A. Tagliacozzo, and A. Trombettoni, *Nuclear Physics B* **909**, 135 (2016).
- [40] D. Giuliano and P. Sodano, *Nuclear Physics B* **770**, 332 (2007).
- [41] D. Giuliano and P. Sodano, *EPL (Europhysics Letters)* **88**, 17012 (2009).
- [42] D. Giuliano and P. Sodano, *Nuclear Physics B* **811**, 395 (2009).
- [43] P.-X. Shen, S. Hoffman, and M. Trif, *Theory of topological spin josephson junctions* (2019), [1912.11458](https://arxiv.org/abs/1912.11458).
- [44] D. Giuliano and I. Affleck, *Journal of Statistical Mechanics: Theory and Experiment* **2013**, P02034 (2013).
- [45] D. Giuliano and I. Affleck, *Phys. Rev. B* **90**, 045133 (2014).
- [46] I. Affleck, J.-S. Caux, and A. M. Zagoskin, *Phys. Rev. B* **62**, 1433 (2000).
- [47] J.-S. Caux, H. Saleur, and F. Siano, *Phys. Rev. Lett.* **88**, 106402 (2002).
- [48] A. Nava, R. Giuliano, G. Campagnano, and D. Giuliano, *Phys. Rev. B* **94**, 205125 (2016).
- [49] A. Nava, R. Giuliano, G. Campagnano, and D. Giuliano, *Phys. Rev. B* **95**, 155449 (2017).
- [50] A. Y. Kitaev, *Physics-Uspekhi* **44**, 131 (2001).

- [51] C. W. J. Beenakker, D. I. Pikulin, T. Hyart, H. Schomerus, and J. P. Dahlhaus, *Phys. Rev. Lett.* **110**, 017003 (2013).
- [52] L. I. Glazman and A. I. Larkin, *Phys. Rev. Lett.* **79**, 3736 (1997).
- [53] A. Cirillo, M. Mancini, D. Giuliano, and P. Sodano, *Nuclear Physics B* **852**, 235 (2011).
- [54] J. Lee and F. Wilczek, *Phys. Rev. Lett.* **111**, 226402 (2013).
- [55] D. Averin and A. Bardas, *Phys. Rev. Lett.* **75**, 1831 (1995).
- [56] P. Coleman, L. B. Ioffe, and A. M. Tsvelik, *Phys. Rev. B* **52**, 6611 (1995).
- [57] D. Giuliano and A. Tagliacozzo, *Journal of Physics: Condensed Matter* **16**, 6075 (2004).
- [58] N. Andrei and C. Destri, *Phys. Rev. Lett.* **52**, 364 (1984).
- [59] I. Affleck and A. W. Ludwig, *Nuclear Physics B* **352**, 849 (1991).
- [60] A. W. W. Ludwig and I. Affleck, *Phys. Rev. Lett.* **67**, 3160 (1991).
- [61] A. Altland, B. Béri, R. Egger, and A. M. Tsvelik, *Journal of Physics A: Mathematical and Theoretical* **47**, 265001 (2014).
- [62] C. Chamon, M. Oshikawa, and I. Affleck, *Phys. Rev. Lett.* **91**, 206403 (2003).
- [63] M. Oshikawa, C. Chamon, and I. Affleck, **2006**, P02008 (2006).
- [64] D. Giuliano and P. Sodano, *New Journal of Physics* **10**, 093023 (2008).
- [65] M. Pino, A. M. Tsvelik, and L. B. Ioffe, *Phys. Rev. Lett.* **115**, 197001 (2015).
- [66] A. M. Tsvelik, *New Journal of Physics* **16**, 033003 (2014).